NASA Technical Paper 1050

Effect of a Simulated Engine Jet Blowing Above an Arrow Wing at Mach 2.0

Barrett L. Shrout and Clyde Hayes

OCTOBER 1977

NASA

NASA Technical Paper 1050

Effect of a Simulated Engine Jet Blowing Above an Arrow Wing at Mach 2.0

Barrett L. Shrout and Clyde Hayes
Langley Research Center
Hampton, Virginia

National Aeronautics
and Space Administration

**Scientific and Technical
Information Office**

1977

SUMMARY

An investigation of the effects of a gas jet simulating a turbojet engine exhaust blowing above a cambered and twisted arrow wing has been conducted in the Langley 4-foot supersonic pressure tunnel at a Mach number of 2.0. Nozzle pressure ratios from 1 (jet off) to as high as 64 were tested with both helium and air used as jet gases. The tests were conducted at angles of attack from -2° to 8° at a Reynolds number of 9.84×10^{6} per meter. Only the forces and moments on the wing were measured.

The results of the investigation indicated that the jet blowing over the wing caused reductions in maximum lift-drag ratio $(L/D)_{max}$ of about 4 percent for helium and 6 percent for air at their respective design nozzle pressure ratios, relative to jet-off data. Moderate changes in the longitudinal, vertical, or angular positions of the jet relative to the wing had little effect on the wing aerodynamic characteristics.

INTRODUCTION

The National Aeronautics and Space Administration has made extensive studies of configurations suitable for application as supersonic cruise vehicles. A part of these studies has been directed toward providing high lift at low speeds. One approach has been to increase the lift by directing the high-velocity exhaust from forward-mounted engines above the upper surface of the wing and flaps. An additional benefit expected from this engine arrangement is reduced noise on the ground because of the shielding of the engine exhaust by the wing. The results of investigations at low speeds of configurations employing engines mounted above the wing for upper surface blowing are reported in references 1 and 2. In addition, references 3 and 4 examine the effects on cruise drag of configurations with nacelles above the wing at high subsonic and transonic speeds.

One of the early proposals for an over-the-wing-blowing engine installation on a supersonic transport configuration consisted of engines mounted on canards ahead of the wing. There was some concern that the beneficial effects on lift at low speeds would be accompanied by a degradation of performance at supersonic speeds.

The purpose of the present investigation was to determine the effects on wing performance at supersonic speeds of an engine exhaust jet simulator mounted forward of a wing and blowing above its upper surface. The variables investigated were angle of attack, nozzle pressure ratio, jet location (vertically and longitudinally), and angle of the jet relative to the wing design plane. In addition, the effects of simulating the engine exhaust jet with both high-pressure helium and high-pressure air were investigated.

SYMBOLS

The models were constructed, wind-tunnel measurements taken, and data reduced by using the U.S. Customary System of Units. Data are presented in the SI System of Units. The force and moment data are referred to the stability axis system. Pitching moment is referenced to a point on the wing root chord 27.3 cm from the wing apex. The symbols are defined as follows:

b	span, 55.48 cm
C_D	drag coefficient, Drag/qS
C_L	lift coefficient, Lift/qS
C_m	pitching-moment coefficient, Pitching moment/$qS\bar{c}$
$\bar{c}$	wing mean aerodynamic chord, 33.02 cm
D	diameter, cm
L/D	lift-drag ratio, C_L/C_D
M	Mach number
$p_{t,j}$	jet total pressure, Pa
$p_{t,j}/p_\infty$	nozzle pressure ratio
p_∞	free-stream static pressure, Pa
q	free-stream dynamic pressure, Pa
S	wing area, half-span model, 0.0687 m^2
V_j	jet velocity, m/sec
w	mass rate of flow, kg/sec
w/ρ	volume flow rate, m^3/sec
y	distance along span, cm
α	angle of attack, deg
γ	ratio of specific heats
ρ	gas density, kg/m^3

Subscripts:

jet	conditions in fully expanded jet
max	maximum

TURBOJET EXHAUST SIMULATION

A turbojet engine exhaust is typically a high-temperature, high-velocity gas jet, with initial plume shape and gas-flow rate determined by nozzle geometry and operating conditions. Ideally, for a wind-tunnel test, the engine exhaust jet would be modeled by duplicating the gas density, pressure, and temperature, matching the nozzle internal and external geometry, and operating the wind tunnel so that the exhaust jet plume shape, velocity, and gas-flow rate were duplicated. For the present investigation, where the jet passes above the upper wing surface, the jet velocity as well as the initial plume shape and gas-flow rate were expected to have the most significant effects on the wing aerodynamic characteristics.

Jet velocity, which is a function of gas temperature, is one of the more difficult parameters to match, generally requires some type of hot-gas generator, and is accompanied by problems of tunnel contamination, corrosion, and hazardous operating conditions. Because of these problems, the use of an unheated gas in the jet simulation would considerably simplify the investigation. Reference 5 contains the results of a study conducted to design wind-tunnel experiments for jet-on effects at both subsonic and supersonic speeds. Although the study was primarily concerned with rocket exhausts, much of the information is applicable to turbojet exhausts. One of the conclusions of the study was that ambient temperature helium could effectively simulate a rocket exhaust with total temperature on the order of 1100 K, which is in the range of turbojet exhaust temperatures. Thus, by using ambient temperature helium, the turbojet exhaust velocity can be simulated, and the internal geometry of the nozzle can be designed so that the initial jet plume shape and flow rate can be simulated in the wind tunnel.

Another gas which is frequently used for turbojet exhaust simulation is cold air. One of its principal drawbacks in simulating a jet exhaust in a wind tunnel at Mach 2.0 is that the maximum jet velocity attainable is not much greater than the free-stream velocity. However, air has the advantages of being plentiful and inexpensive and is without the disadvantage of tunnel contamination which occurs with helium. And, like the nozzle designed for helium, the nozzle designed for air can duplicate the initial plume shape and flow rate of the turbojet exhaust.

MODEL AND APPARATUS

Sketches of the test setup are presented in figure 1. A semispan wing model was attached to a four-component strain-gage balance set in a horizontal splitter plate which was in turn mounted to the permanent tunnel sting. To prevent fouling, a gap of 0.025 to 0.037 cm was maintained between the wing root and the splitter plate, except where the wing stub was attached to the balance. Boundary-layer transition on the wing was fixed by a strip of no. 60 carborundum grit located near the leading edge.

The nonmetric jet-flow model was rigidly attached to the splitter plate and connected to the high-pressure gas supplies through a fitting on the underside of the splitter plate. A thermocouple located within this fitting measured the gas temperature while a total pressure tube located in the simulator just forward of the nozzle measured jet total pressure. The extended axis of the jet-flow model nozzle passed over the wing at a spanwise location of $0.247y/(b/2)$.

Angle of attack for the wing and jet-flow model was varied by yawing the sting-splitter plate combination. Angle of attack was measured during tunnel operation by observing a prism mounted in the wing through a spectrometer.

Details of the wing are shown in figure 2. The semispan wing model is an arrow wing with a leading-edge sweep angle of 70°. It has a 3-percent circular-arc airfoil section from root to tip. The wing is twisted and cambered for a design lift coefficient of 0.08 at a Mach number of 2.0. This wing is the same as wing 2 of reference 6, and details of the camber surface ordinates may be found in that reference.

Details of the canard, flow-through nacelle, jet-flow model, and the various nozzles used in the test are shown in figure 3. The canard and flow-through nacelle models were included in the test program to determine the effect of the individual components of the jet-flow model on the wing aerodynamic characteristics. The external lines of the canard and canard supports for the flow-through nacelle and jet-flow model were identical. The convergent-divergent regions of the primary, canted, and extended nozzles were also identical. Design of the jet simulator used in these tests included the following parameters: mass rate of flow, which can be scaled from some representative aircraft size and operating conditions; initial shape of the exhaust plume, which can be achieved by appropriate nozzle pressure ratio, depending on the gas specific heat ratio; and jet velocity, which was initially achieved by using helium as the jet gas.

The helium nozzle geometric characteristics were determined from the ratio of the model wing reference area to a full-sized aircraft with a reference area of 836 m^2. The aircraft engine was assumed to be a turbojet with a static sea-level airflow of 408.15 kg/sec. It was further assumed that the aircraft was operating at a Mach number of 2.0 at an altitude of approximately 19 800 m where the engine airflow rate would be 86.16 kg/sec. The scaled gas mass flow rate is 0.01417 kg/sec for the engine simulator using helium. In addition to the scaled mass flow rate, the nozzle was designed to produce the same initial plume shape as that of a turbojet engine. In reference 7, data are presented that show the nozzle pressure ratio required for cold air ($\gamma = 1.4$) to produce the same initial plume shape as for an afterburning turbojet ($\gamma = 1.27$). A linear variation of nozzle pressure ratio was assumed; and for helium ($\gamma = 1.66$), the required nozzle pressure ratio at $M = 2.0$ is 21.4. The nozzle exit size was determined by assuming that the flow should expand to a value that was twice the free-stream static pressure at the exit face. The wind-tunnel static pressure was assumed to be 16.547 kPa, whereas the reservoir temperature for the gas supply was assumed to be room temperature (294.44 K). Under these conditions, the volume flow rate at the exit face was calculated to be 0.1015 m^3/sec.

However, the wind-tunnel tests using helium as the jet gas were conducted with a wind-tunnel test-section static pressure of 11.059 kPa. The volume flow rate at the exit face for helium at the design nozzle pressure ratio was thus 0.1308 m^3/sec.

The air nozzle, which was designed subsequent to the helium gas tests, was based on the following parameters. The volume flow rate at the exit face was 0.1308 m^3/sec to match the actual helium jet test conditions with a free-stream

static pressure of 11.059 kPa. The required nozzle pressure ratio to match the initial plume shape (from ref. 5) was 15.4, and the jet flow was assumed to expand to a value that was twice the free-stream static pressure at the exit face. The gas reservoir was again assumed to be at room temperature.

TEST CONDITIONS

The tests were conducted in the Langley 4-foot supersonic pressure tunnel at a Mach number of 2.0. Tunnel total pressure was 87.356 kPa and total temperature was 316.67 K. Reynolds number was 9.84×10^6 per meter. The free-stream velocity in the test section was computed to be 535.79 m/sec. Angle of attack was varied from -2° to 8° for all the test configurations. The helium jet-flow tests were conducted for nozzle pressure ratios of 1 (jet off), 16, 32, and 48. The air jet-flow tests using the helium nozzles were conducted for nozzle pressure ratios of 1, 16, 32, 48, and 64. For the air jet-flow tests using the air nozzle, the maximum nozzle pressure ratio was limited to 32 by the size of the supply lines. Some of the theoretical jet-flow parameters for isentropic fully expanded flow are presented in table I.

TABLE I.- THEORETICAL JET FLOW CONDITIONS, ISENTROPIC, FULLY EXPANDED

[All theoretical jet data are based on a jet total temperature of 294 K. For the helium tests, jet total temperature varied between 286 K and 299 K. For the air tests, jet total temperature varied between 286 K and 297 K.]

$P_{t,j}/P_\infty$	$P_{t,j}$, kPa	Helium gas; helium nozzle			Air gas; helium nozzle			Air gas; air nozzle		
		V_j, m/sec	w/ρ, m^3/sec	Plume diameter, cm	V_j, m/sec	w/ρ, m^3/sec	Plume diameter, cm	V_j, m/sec	w/ρ, m^3/sec	Plume diameter, cm
16	172.37	1431	0.1323	1.08	586	0.0636	1.18	586	0.2209	2.19
32	344.74	1514	.2011	1.30	609	.1042	1.48	609	.3620	2.75
48	517.10	1551	.2566	1.45	628	.1393	1.68	628	.4840	3.13
64	689.47	1574	.3050	1.57	640	.1710	1.84	640	.5941	3.44

The range of jet-on nozzle pressure ratios varied from near the design point to well above it. Thus, the effects of some variation in jet velocity and considerable variation in volume flow rate could be evaluated for the various nozzle and gas combinations. Note that for helium, the maximum jet velocity was nearly three times the tunnel free-stream velocity, whereas for air the maximum jet velocity was only about 20 percent greater than the tunnel free-stream velocity.

Contamination of the tunnel airstream during the helium tests was of major concern. Between each run, consisting of a range of nozzle pressure ratios at one angle of attack, the tunnel was operated for approximately 30 min with maximum exchange of air. After two runs, a tunnel air sample was analyzed with a mass spectrometer. The maximum contamination allowable was arbitrarily set at 2 percent and data from runs that were found to exceed that limit were not used.

PRESENTATION OF RESULTS

The results of this investigation are shown in the following figures:

DISCUSSION OF RESULTS

Details of the jet plume downstream of the nozzle exit are shown in figure 4. Some of the theoretical characteristics of the plume as a function of nozzle pressure ratio are shown in figure 4(a). For both gases, the velocity change is relatively small for a substantial variation of nozzle pressure ratio. The theoretical plume sizes increase about 30 percent for helium and about 40 percent for air over the nozzle pressure range shown. The schlieren photographs in figure 4(a) are for the primary helium nozzle, using helium as the jet fluid, and with the tunnel at the test operating conditions. The photographs show that there is a rapid expansion of the plume just aft of the exit face, and as the plume continues downstream, it grows in size to about 3 cm (about 3 primary nozzle exit diameters) and the jet plume boundaries become less well-defined, probably because of some decay in jet velocity and mixing with the tunnel flow. It can be seen from the sketch of the wing-nacelle profile in figure 4(b) that even the largest plume pictured for a nozzle pressure ratio of 48 would still pass above the upper wing surface for the straight nozzles at $\alpha = 0^{\circ}$; for angles of attack greater than 0°, the tunnel flow would tend to turn the plume away from the wing.

During calibration of the air supply system, the primary helium nozzle in the lower position was operated at various jet pressures with the tunnel air flow off and the tunnel at ambient pressure and temperature. No discernible effects of the jet acting on the wing were measured under these conditions. It can be concluded that for the primary and extended nozzles, using either air or helium, the jet plume did not impinge on the wing surface; thus, it would appear that any jet effects measured on the wing when testing the primary or extended nozzles would be primarily due to interference between the jet plume and the wing flow field.

For the canted nozzle in the lower position, an extension of the nozzle axis passes within 1.5 primary nozzle exit diameters of the wing. Thus, for the canted nozzle in the lower position, the exhaust plume might be expected to impinge on the wing surface if it is unaffected by the tunnel free stream and the wing flow field. For the air nozzle, the plume is larger than that for the helium nozzles to maintain a similar volume flow rate, and the undisturbed plume may have impinged on the upper wing surface, particularly from the lower nacelle position.

The effects of the canard, flow-through nacelle, and primary helium nozzle jet simulator (jet off) on the wing are shown in figure 5. At angles of attack below 0°, the canard and nacelle components produce an upwash over the wing. The effect of the upwash on the twisted and cambered wing is to increase lift and produce a thrust component on the wing, which reduces drag. The increase in lift is slightly greater for the lower canard position whereas the decrease in drag is greater for the upper canard position. At angles of attack above 0°, the canard and nacelle components produce a downwash over the wing which reduces lift and increases drag due to lift because of an adverse effect on the wing lift distribution. These effects were larger for the lower canard position.

The pitching moment near zero lift increased because of both upper and lower canard installations. For the lower canard position, the wing center of lift moved slightly aft, with a consequent increase in the stability level. The slight pitch-up tendency of the wing alone at the highest lift coefficients was somewhat modified by the canard and nacelle components in both the upper and lower positions.

Helium

The effect of the helium jet flow from the upper position for the primary, extended, and canted nozzles is shown in figure 6. Increasing the nozzle pressure ratio at all angles of attack resulted in slight decreases in lift and slight increases in pitching moment. At the higher angles of attack, drag decreased slightly with increased nozzle pressure ratio. However, when pitching-moment and drag coefficients are plotted against lift coefficient, as shown in figure 6, the result of the lift loss is an increase in drag and a decrease in pitching moment with increasing nozzle pressure ratio. The $(L/D)_{max}$ was decreased about 4 percent by operation of the helium jet at a nozzle pressure ratio near the design pressure ratio of 21. The effects of varying nozzle pressure ratio for primary, extended, and canted nozzles for the lower position, shown in figure 7, were essentially the same as those for the upper position.

The effect of vertical nacelle position and nozzle pressure ratio is shown in figure 8. The data are for $\alpha = 2^{\circ}$ which is near the angle of attack for $(L/D)_{max}$. The increments in the data for the upper and lower positions are essentially constant with changes in nozzle pressure ratio. For this angle of attack, C_m and C_D show little variation with increasing nozzle pressure ratio, whereas C_L decreases slightly. For the upper position, C_L is consistently greater and C_D is consistently less than that for the corresponding lower position data. Note that these differences are due to the canard-nacelle location relative to the wing and are not due to jet effects.

A comparison between the primary and extended helium nozzles for various nozzle pressure ratios is shown in figure 9. The extended nozzle was included in the test program to determine whether there was any sensitivity to changes in the longitudinal position of the jet. There was essentially no difference in the data for the primary and extended nozzles in either the upper or lower position.

The effect of nozzle cant is shown in figure 10. The nozzle was angled so that the jet plume would pass closer to the upper surface of the wing. Except for a slightly greater decrease in lift coefficient at the higher nozzle pressure ratios and a consequent decrease in L/D, there was essentially no difference in the data from the tests of the canted and primary nozzles.

For the canted nozzle in the lower position, where the plume was expected to impinge on the wing, these results indicate that the direct effect of the plume on the wing was negligible or that the tunnel free stream and wing flow field turned the plume so that it did not impinge on the wing surface.

Air

Because contamination of the tunnel airstream with helium was a problem, and because of the cost of helium, the effects of substituting air for helium as the jet fluid were investigated. Air blowing tests were conducted by using the primary and extended helium nozzles and by using a nozzle designed for air. The effect on the wing of the various nozzles using air for the jet exhaust for the upper position is shown in figure 11. The gross effects for air in the helium nozzles are smaller than those for the helium gas data in figure 6. There is a very slight decrease in lift with increasing nozzle pressure ratios; however, the drag decrease noted in the helium gas data at large values of lift coefficient does not appear in the air jet data. As a consequence, the variations of L/D with nozzle pressure ratio and lift coefficient are similar for both helium and air. The results for the air nozzle (fig. 11(c)), which had the highest flow rate and largest plume diameter of the nozzles tested (see table I and fig. 4), are similar to the results for air in the helium nozzles although of greater magnitude. The $(L/D)_{max}$ was decreased about 6 percent by the air jet operating at a nozzle pressure ratio near the design pressure ratio of 15.

Data for air jet flow in the lower position are shown in figure 12. The variation of the data with changes in nozzle pressure ratio is much the same as that for the data for the upper position, although smaller in magnitude.

A comparison of the air jet data for the upper and lower nacelle positions for an angle of attack of 2° is shown in figure 13. In figure 13(a), for the primary nozzle, the increments between the data for upper and lower positions are essentially constant for the various nozzle pressure ratios; thus, the difference is due to the position of the canard nacelle rather than the position of the jet relative to the wing. The air nozzle data in figure 13(b) show a slight effect of the position of the jet, the drag for the upper nacelle position increasing more rapidly with increasing nozzle pressure ratio than that for the drag for the lower position.

Comparison of Air and Helium as Exhaust Gas Simulators

The effect of the type of jet gas used on the wing aerodynamic characteristics is shown in figure 14 as a function of nozzle pressure ratio. These data are again for $\alpha = 2°$, which is near the angle of attack for $(L/D)_{max}$. Only minor changes occurred in the wing aerodynamic characteristics because of the switching from helium to air as the jet gas for the upper position and these changes were even less pronounced for the lower position. The changes that did occur can be attributed to a combination of the jet velocity difference and a difference in plume size which is directly related to volume flow rate. An evaluation of the effect of volume flow rate can be made by comparing the data for the primary nozzle and the air nozzle in figure 14, both using air as the jet gas, because for any nozzle pressure ratio, both nozzles have the same theoretical velocity. The primary effects associated with the higher volume flow rate (larger plume size) of the air nozzle are an increase in wing drag (resulting in a loss in L/D) and an increase in negative pitching moment.

The effect of jet velocity on the wing aerodynamic characteristics from the upper nacelle position is shown in figure 15. The data are extracted from figure 14(a) by using the theoretical jet plume data from figure 4(a). The scales in figure 15 are greatly expanded for clarity. The symbols on the right side of the figure represent data for the primary nozzle using helium, whereas the symbols on the left side of the figure represent data for the primary nozzle using air. Each pair of symbols shows the effect of a change in jet velocity, plume diameter being held constant. The effects of increasing jet velocity at constant plume diameter include a reduction in negative pitching moment and a decrease in lift and drag, with a net loss in L/D. With the exception of drag, the effects of increased jet velocities are magnified as plume diameter is increased, as indicated by the steeper slopes of the lines connecting the data points for the larger plume diameters.

CONCLUDING REMARKS

Forces and moments were measured on a twisted and cambered wing at a Mach number of 2.0 in the presence of a turbojet exhaust simulator, using both helium and air, blowing above the upper surface of the wing. Because the jet plume did not impinge the wing surface during most of the tests, the primary effects measured on the wing were due to interference between the jet plume and the wing flow field.

The jet-off effect of the canard and nacelle components was to produce an upwash on the wing for angle of attack α of 0°, which increases lift and reduces drag. Above $\alpha = 0°$, the downwash produced by the canard and nacelle components reduced lift and increased drag due to lift.

For the jet-on tests, the effect of increasing the nozzle pressure ratio was a reduction in maximum lift-drag ratio $(L/D)_{max}$. For nozzle pressure ratios required to match the turbojet exhaust plume shape (approximately 15 for air and 21 for helium), both gases had similar effects on the wing aerodynamic characteristics; as a result, there was a loss in $(L/D)_{max}$ of about 4 percent for helium and 6 percent for air, relative to the jet-off data. Moderate changes in the longitudinal, vertical, or angular position of the jet relative to the wing had little effect on the wing aerodynamic characteristics.

For an angle of attack of 2° (near that for $(L/D)_{max}$), the effects of increasing volume flow rate (increased plume size) at constant velocity were an increase in wing drag, essentially no change in lift, and a decrease in pitching moment. Increasing jet velocity, with the jet plume diameter held constant, reduced drag and lift and produced a net loss in L/D.

Langley Research Center
National Aeronautics and Space Administration
Hampton, VA 23665
September 2, 1977

REFERENCES

1. Coe, Paul L., Jr.; McLemore, H. Clyde; and Shivers, James P.: Effects of Upper-Surface Blowing and Thrust Vectoring on Low-Speed Aerodynamic Characteristics of a Large-Scale Supersonic Transport Model. NASA TM X-72792, 1975.

2. Shivers, James P.; McLemore, H. Clyde; and Coe, Paul L., Jr.: Low-Speed Wind Tunnel Investigation of a Large-Scale Advanced Arrow Wing Supersonic Transport Configuration With Engines Mounted Above the Wing for Upper Surface Blowing. NASA TM X-72761, 1975.

3. Reubush, David E.: An Investigation of Induced Drag Reduction Through Over-the-Wing Blowing. AIAA Paper No. 77-884, July 1977.

4. Mercer, Charles E.; and Carson, George T., Jr.: Upper Surface Nacelle Influence on SCAR Aerodynamic Characteristics at Transonic Speeds. Proceedings of the SCAR Conference - Part 1, NASA CP-001, [1977], pp. 137-154.

5. Li, T. Y.; Yoler, Y. A.; and Morgan, A. J. A.: The Design of Wind Tunnel Experiments for the Study of Jet-On Effects. NAVORD Rep. 3473 (NOTS 1081), U.S. Naval Ord. Test Station (China Lake, Calif.), Apr. 12, 1955.

6. Carlson, Harry W.: Aerodynamic Characteristics at Mach Number 2.05 of a Series of Highly Swept Arrow Wings Employing Various Degrees of Twist and Camber. NASA TM X-332, 1960.

7. Norton, Harry T., Jr.; Foss, Willard E., Jr.; and Swihart, John M.: An Investigation of Modified Clustered Jet-Exit Arrangements at Supersonic Speeds. NASA TM X-540, 1961.

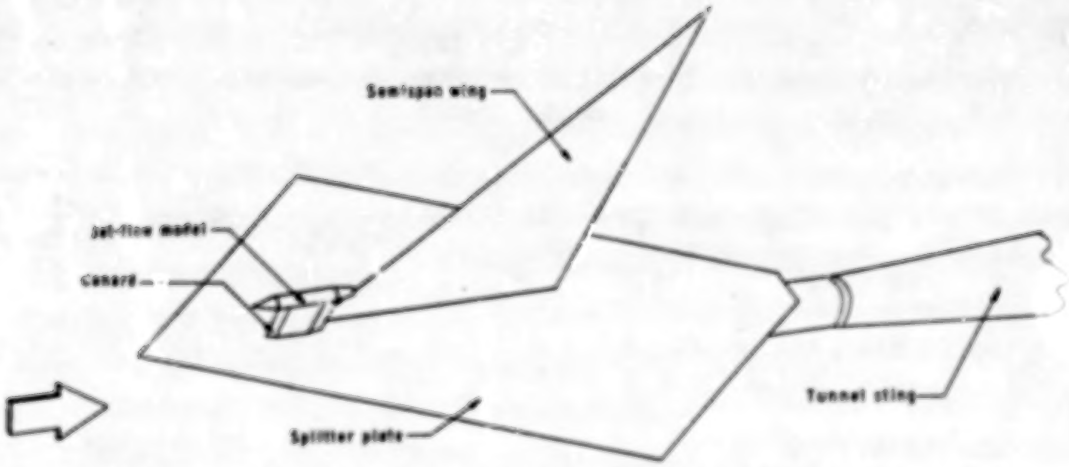

(a) Test rig in tunnel. Upper surface of splitter plate is parallel to tunnel flow.

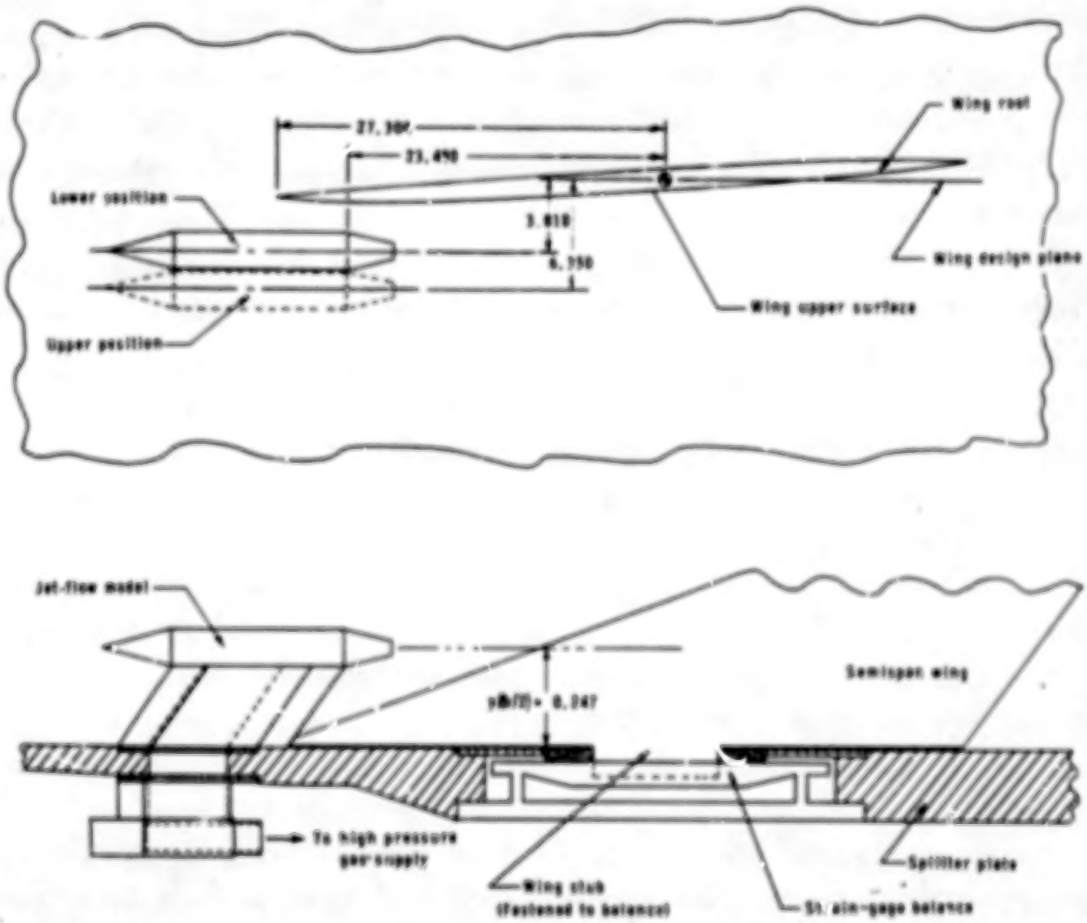

(b) Plate-balance-model details.

Figure 1.- Sketch of test setup. All dimensions are in centimeters.

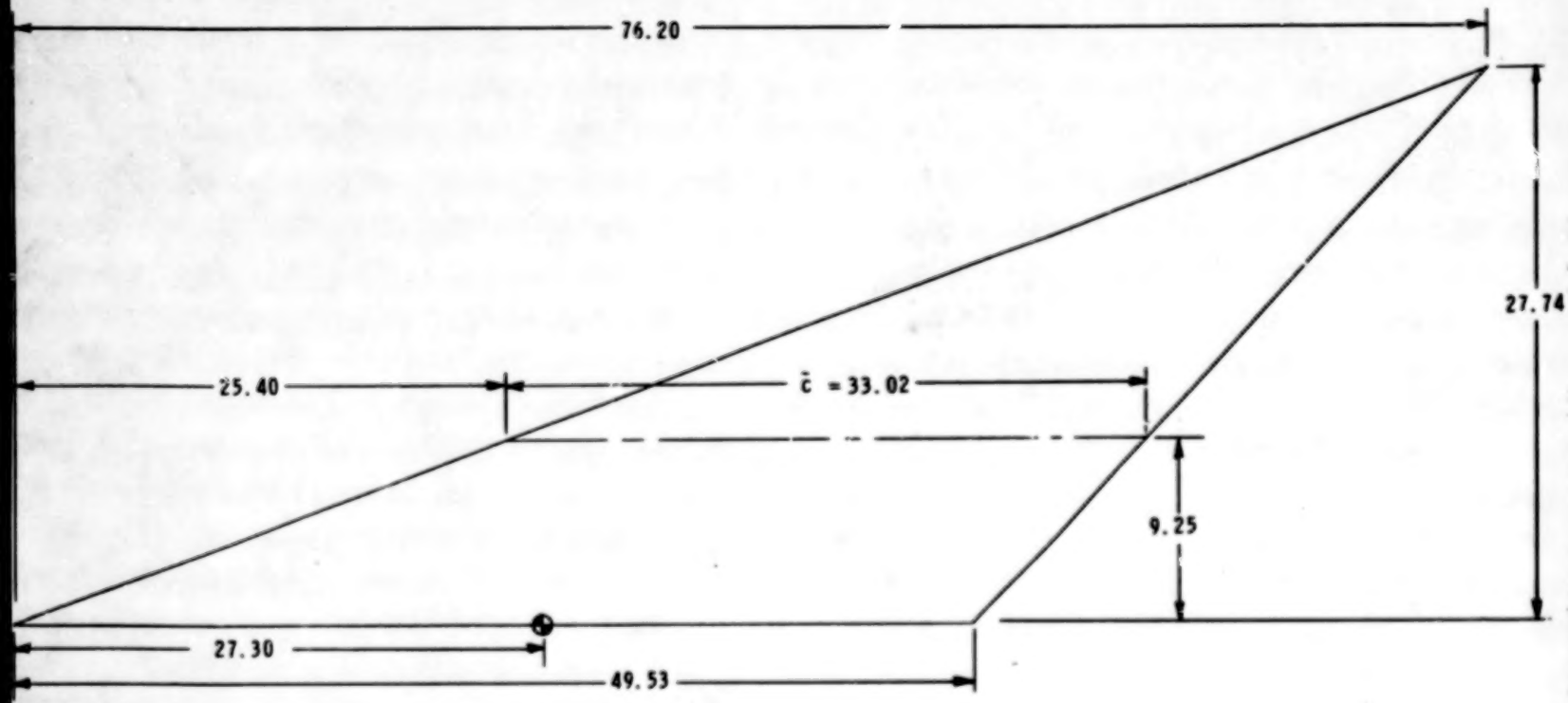

Figure 2.- Sketch of wing model. All dimensions are in centimeters.

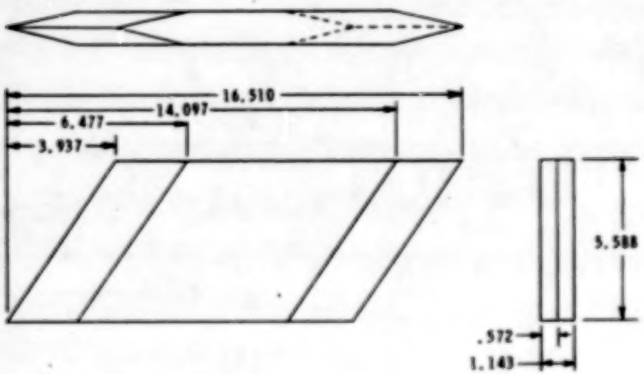

Canard

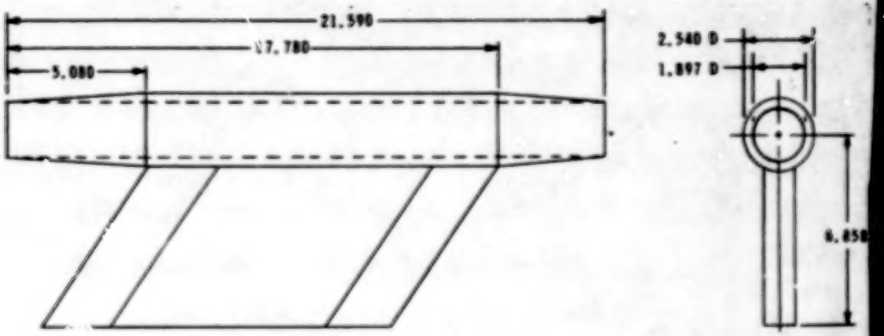

Flow-through nacelle

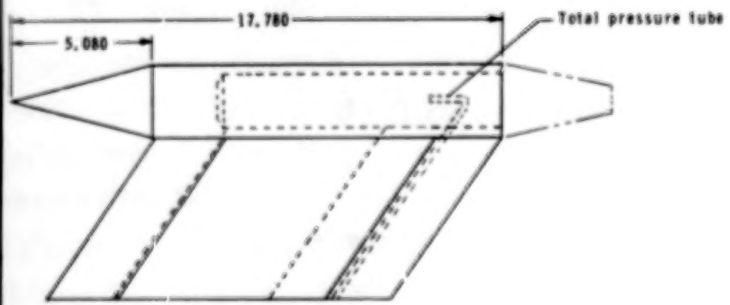

Jet-flow model

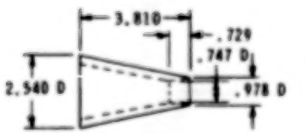

Primary nozzle
This section of nozzle is identical on the canted and extended nozzles

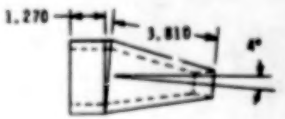

Canted nozzle

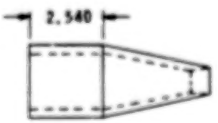

Extended nozzle

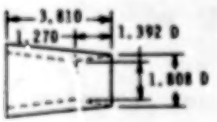

Air nozzle

Figure 3.- Details of canard, flow-through nacelle, and jet flow model.
All dimensions are in centimeters.

(a) Schlieren photographs of primary nozzle helium jet exhaust plume. Wing not installed.

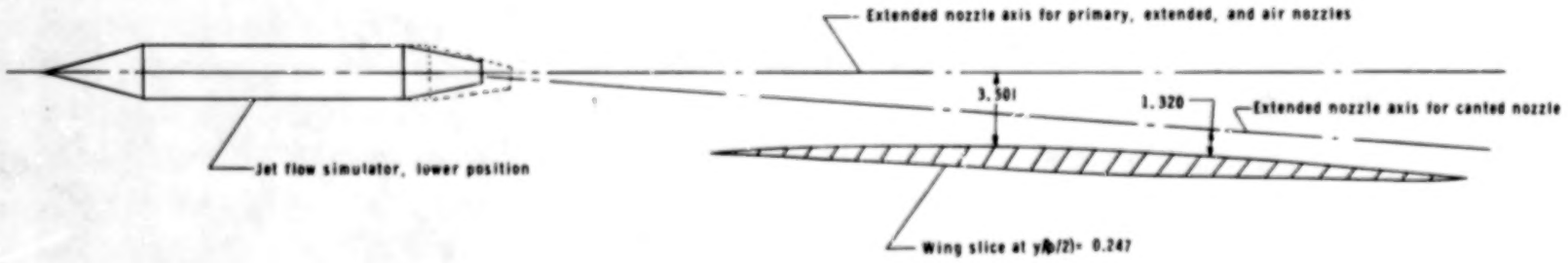

(b) Profile sketch of model installation showing extended nozzle axes. View is normal to splitter plate, looking outboard. All linear dimensions are in centimeters.

Figure 4.- Jet exhaust downstream of nozzle exit.

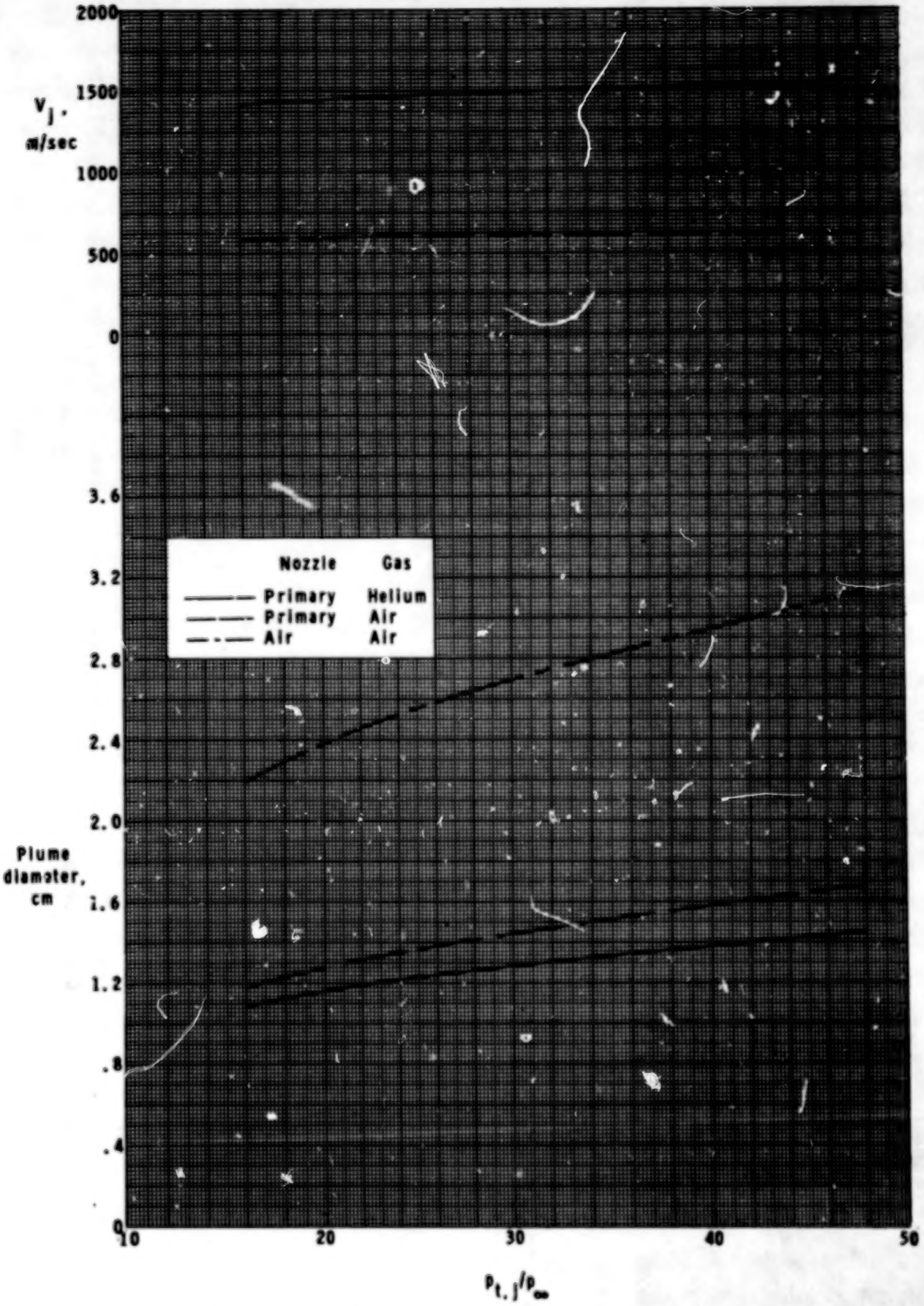

(c) Theoretical jet velocity and plume diameter as a function of nozzle pressure ratio, fully expanded flow.

Figure 4.- Concluded.

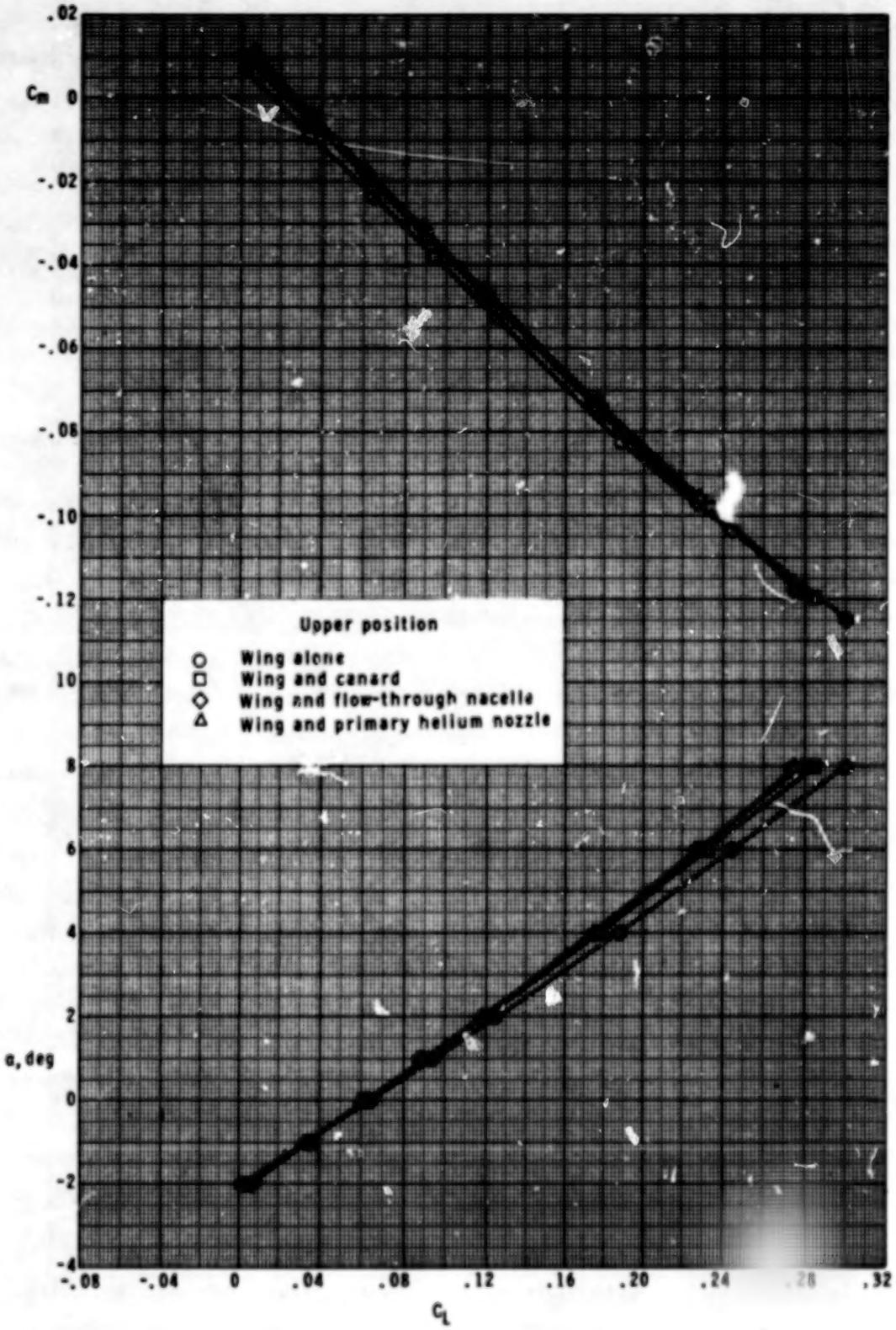

(a) Upper position.

Figure 5.- Effect of canard, flow-through nacelle, and primary nozzle, jet off, on longitudinal aerodynamic characteristics of wing.

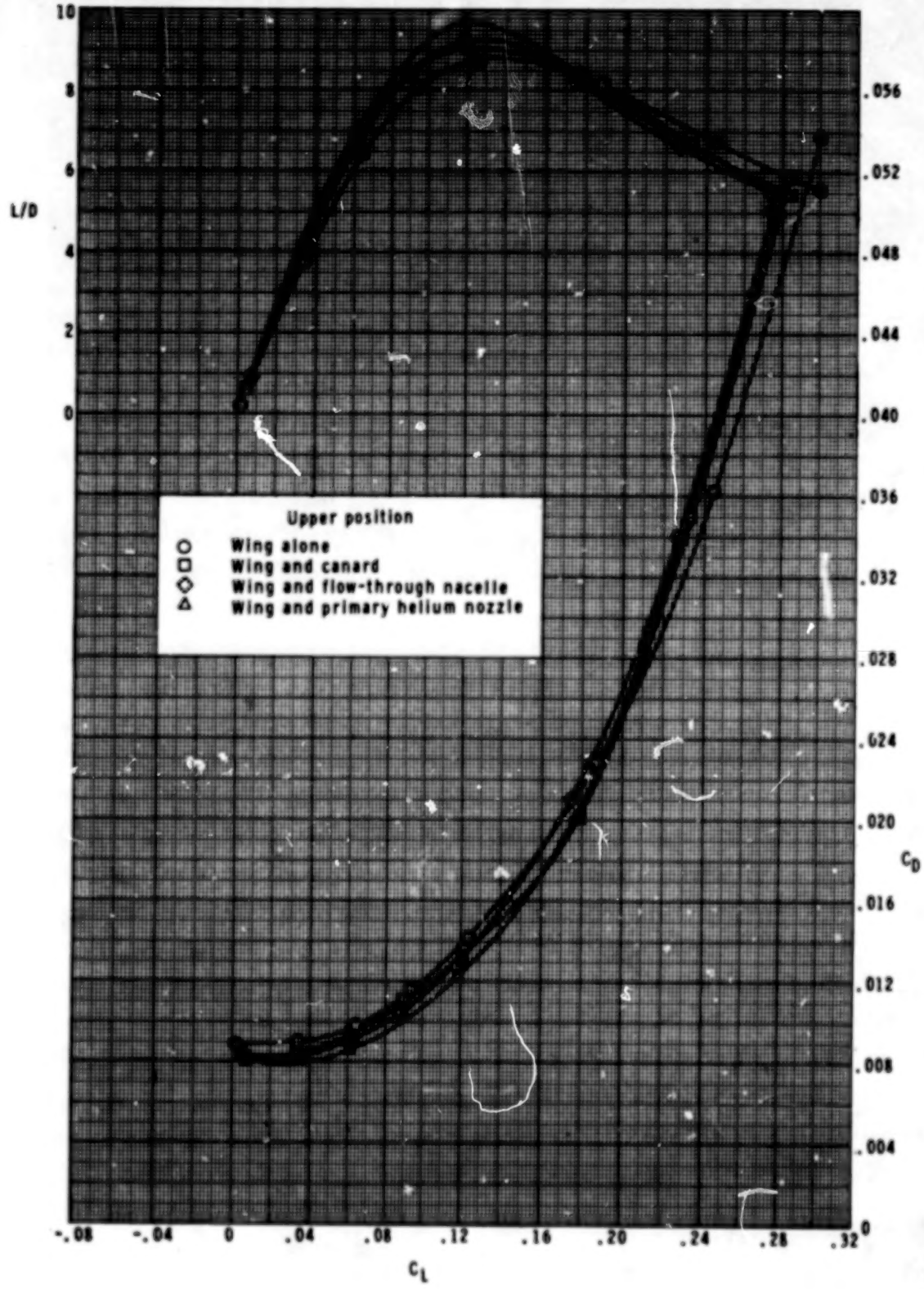

(a) Concluded.

Figure 5.- Continued.

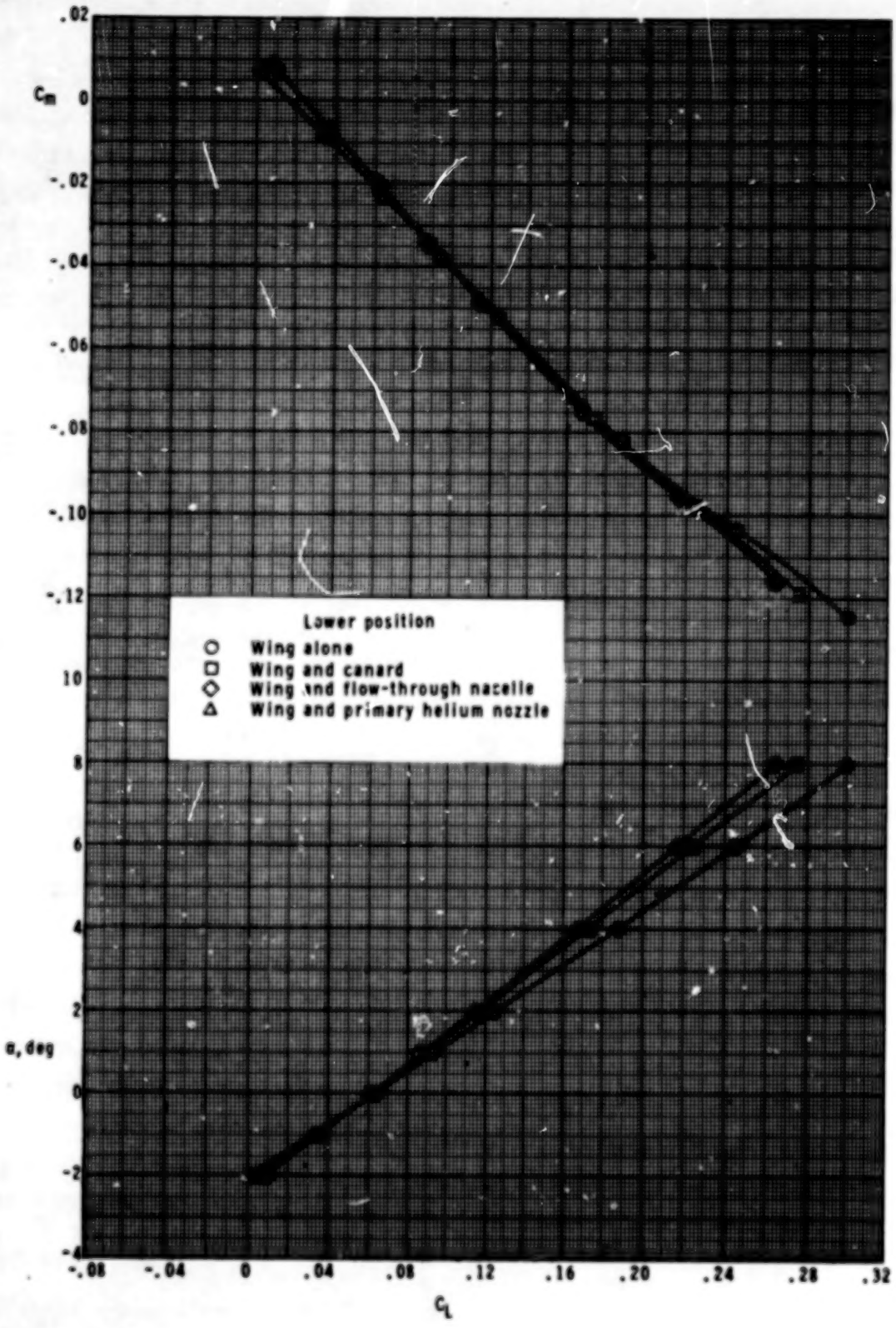

(b) Lower positions.

Figure 5.- Continued.

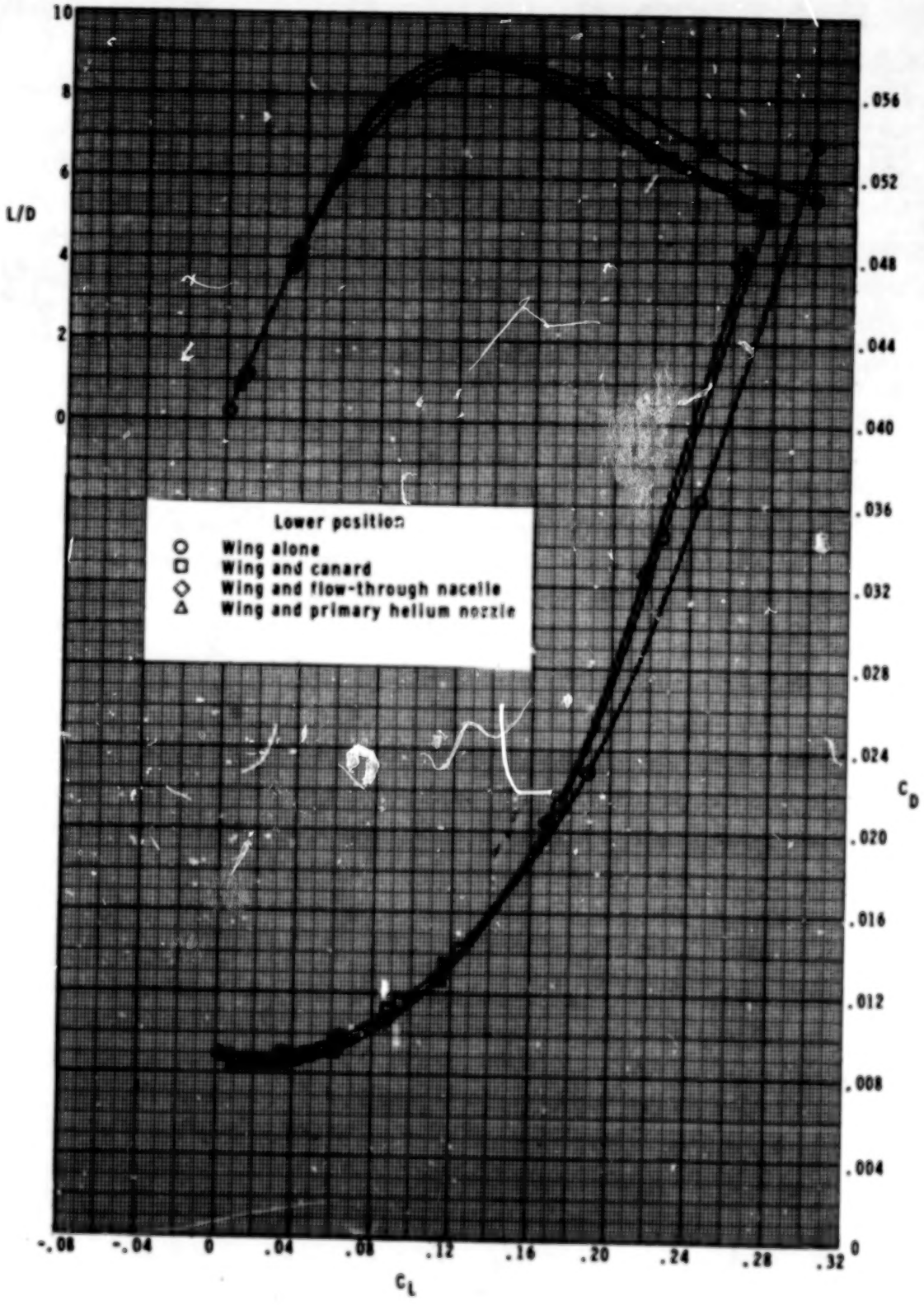

(b) Concluded.

Figure 5.- Concluded.

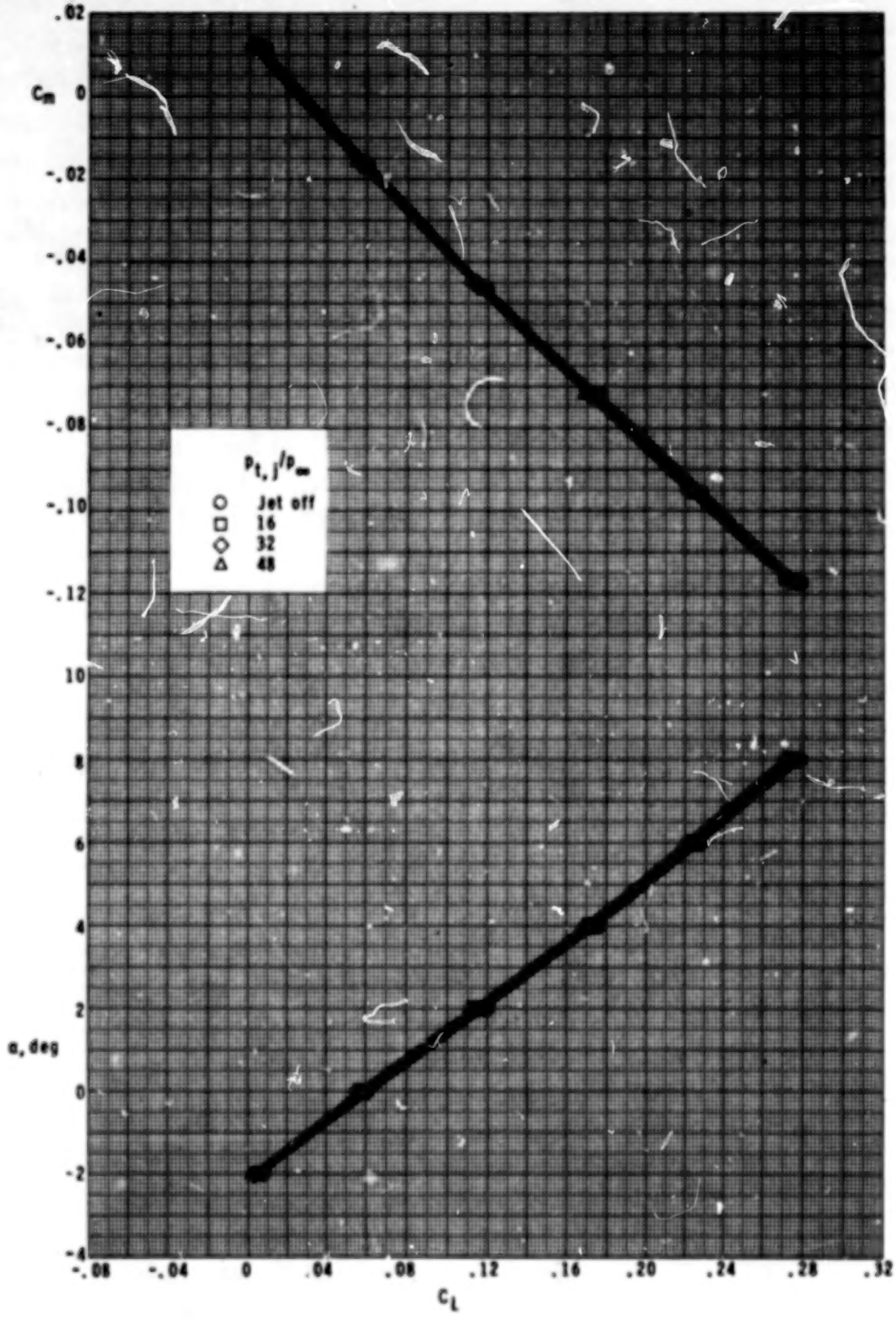

(a) Primary nozzle.

Figure 6.- Effect of helium jet flow on longitudinal aerodynamic characteristics of wing. Upper nacelle position.

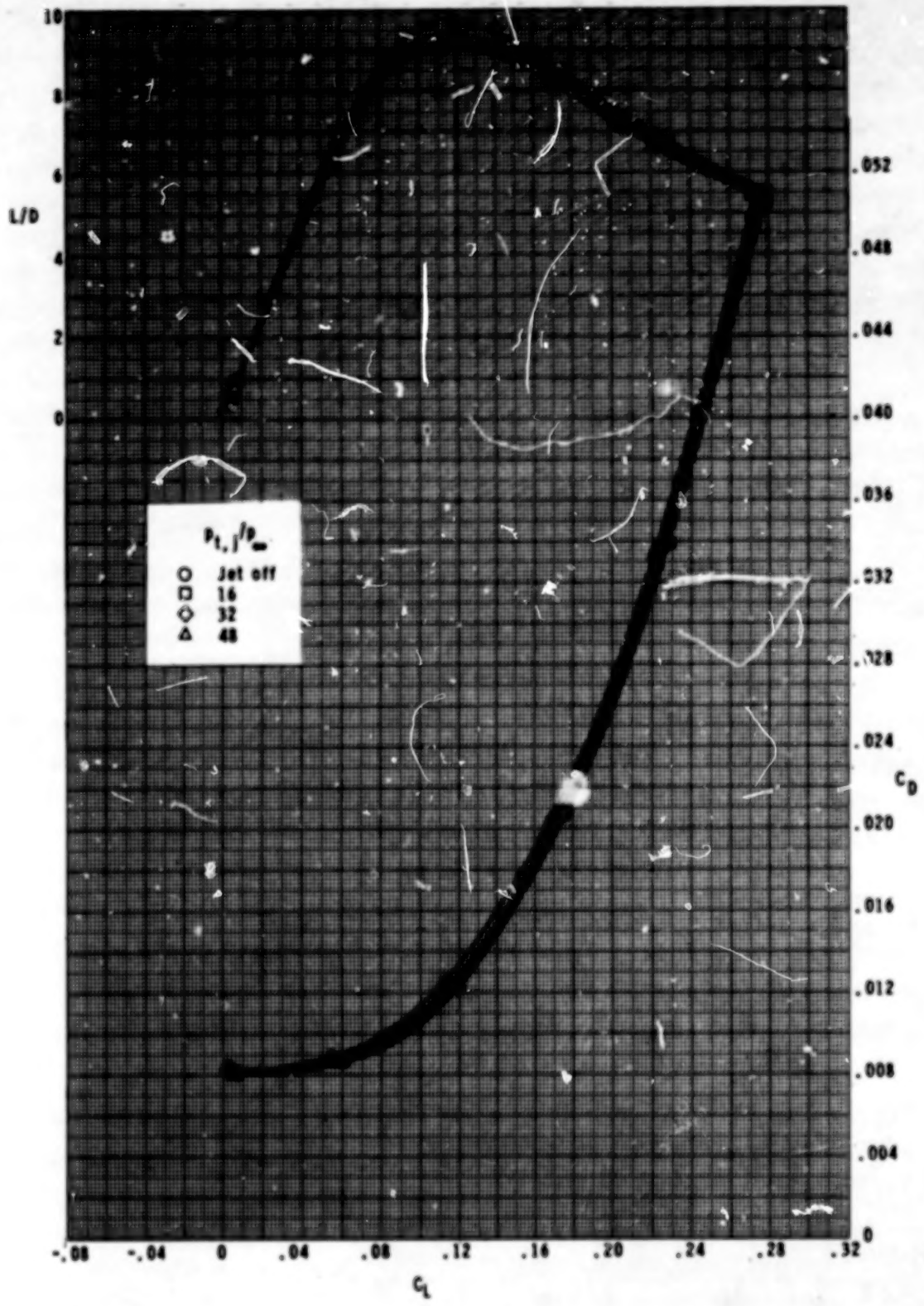

(a) Concluded.

Figure 6.- Continued.

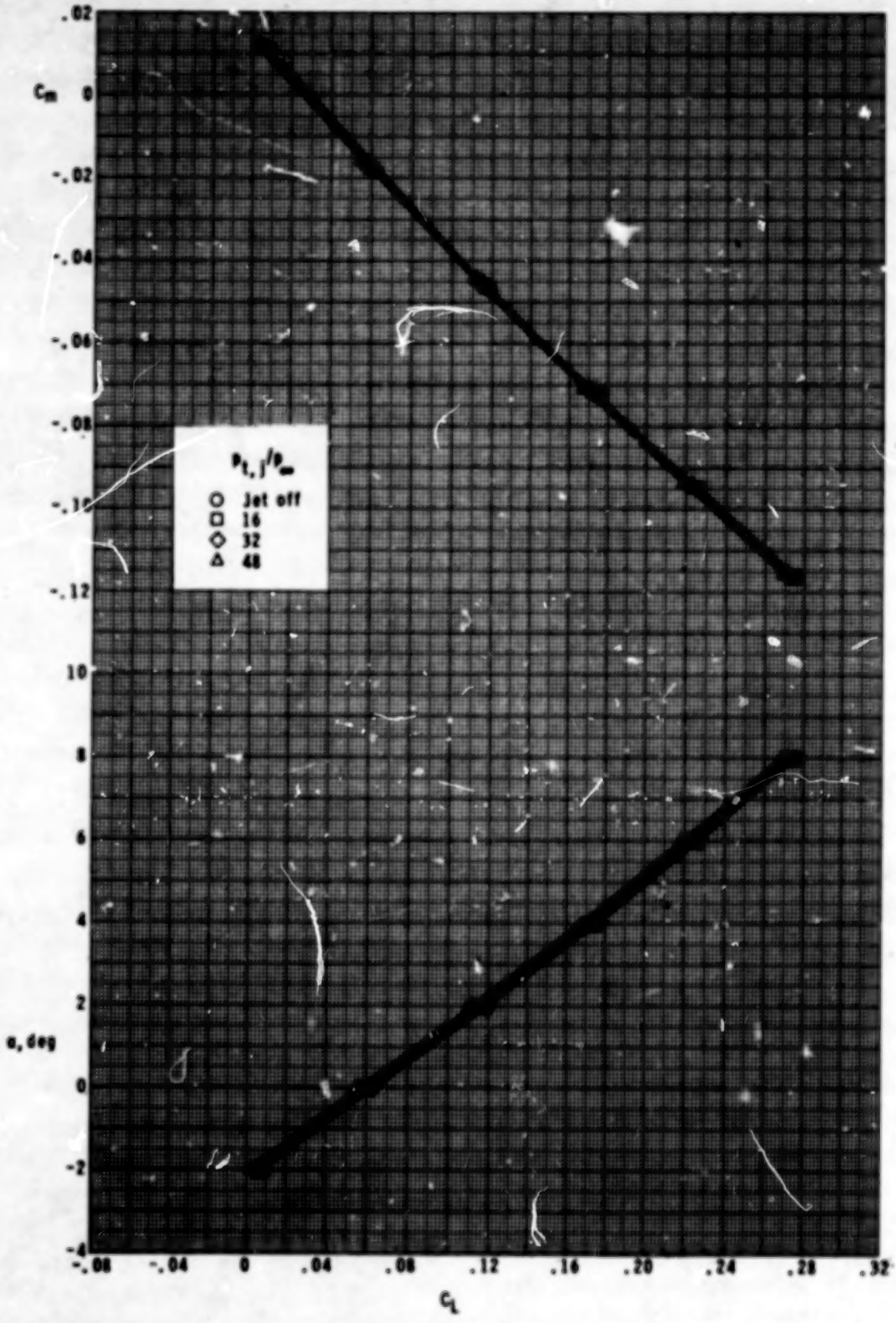

(b) Extended nozzle.

Figure 6.- Continued.

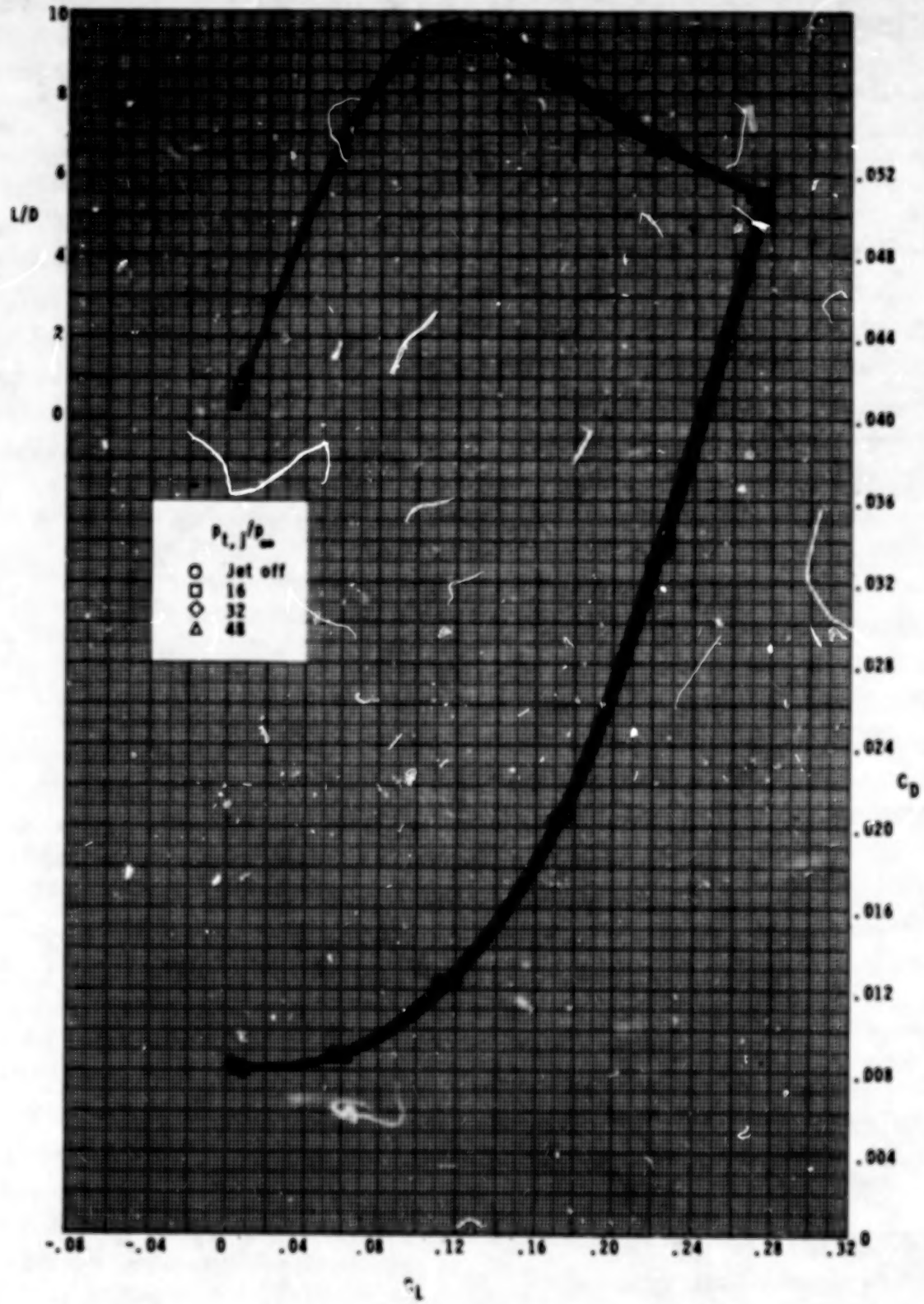

(b) Concluded.

Figure 6.- Continued.

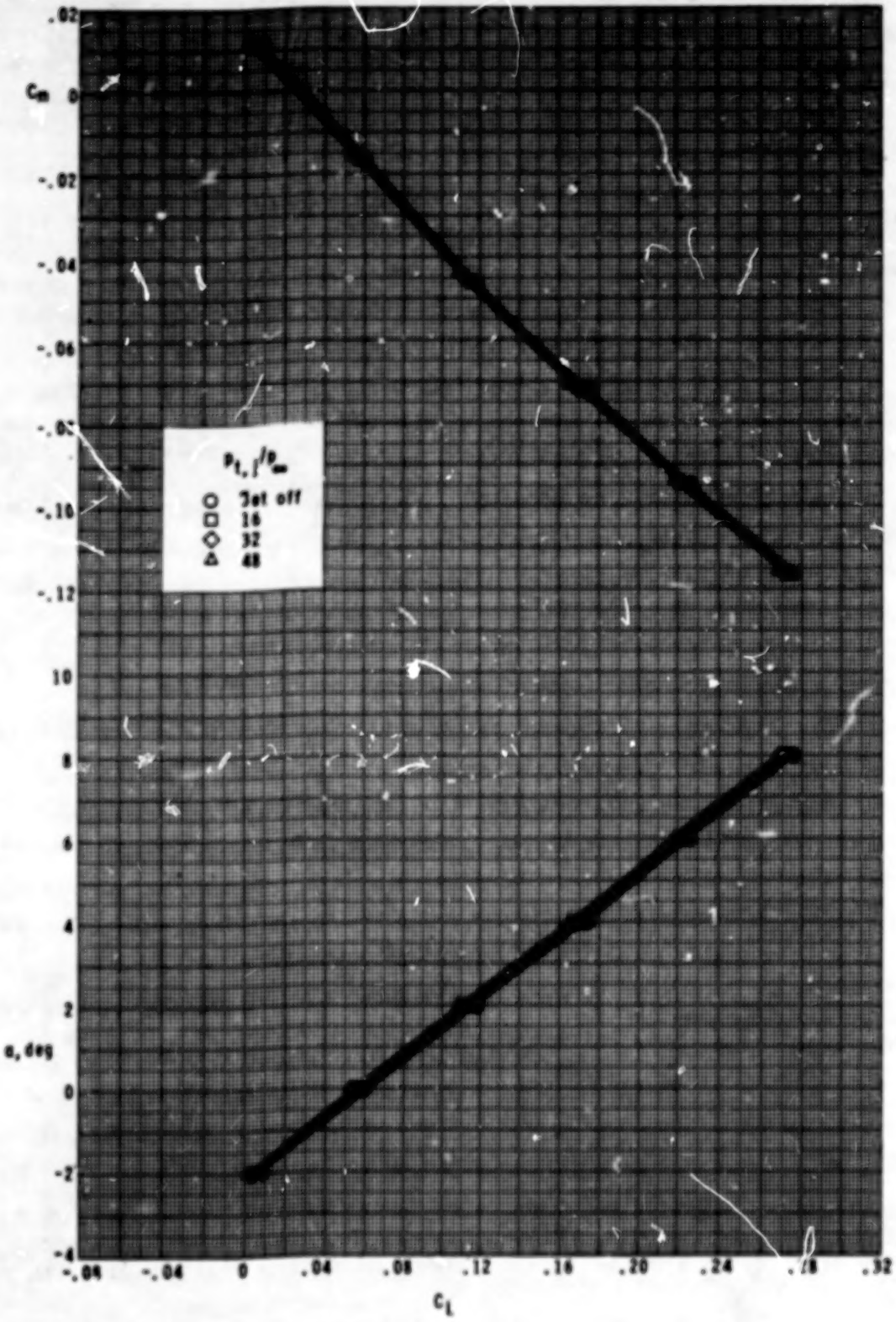

(c) Canted nozzle.

Figure 6.- Continued.

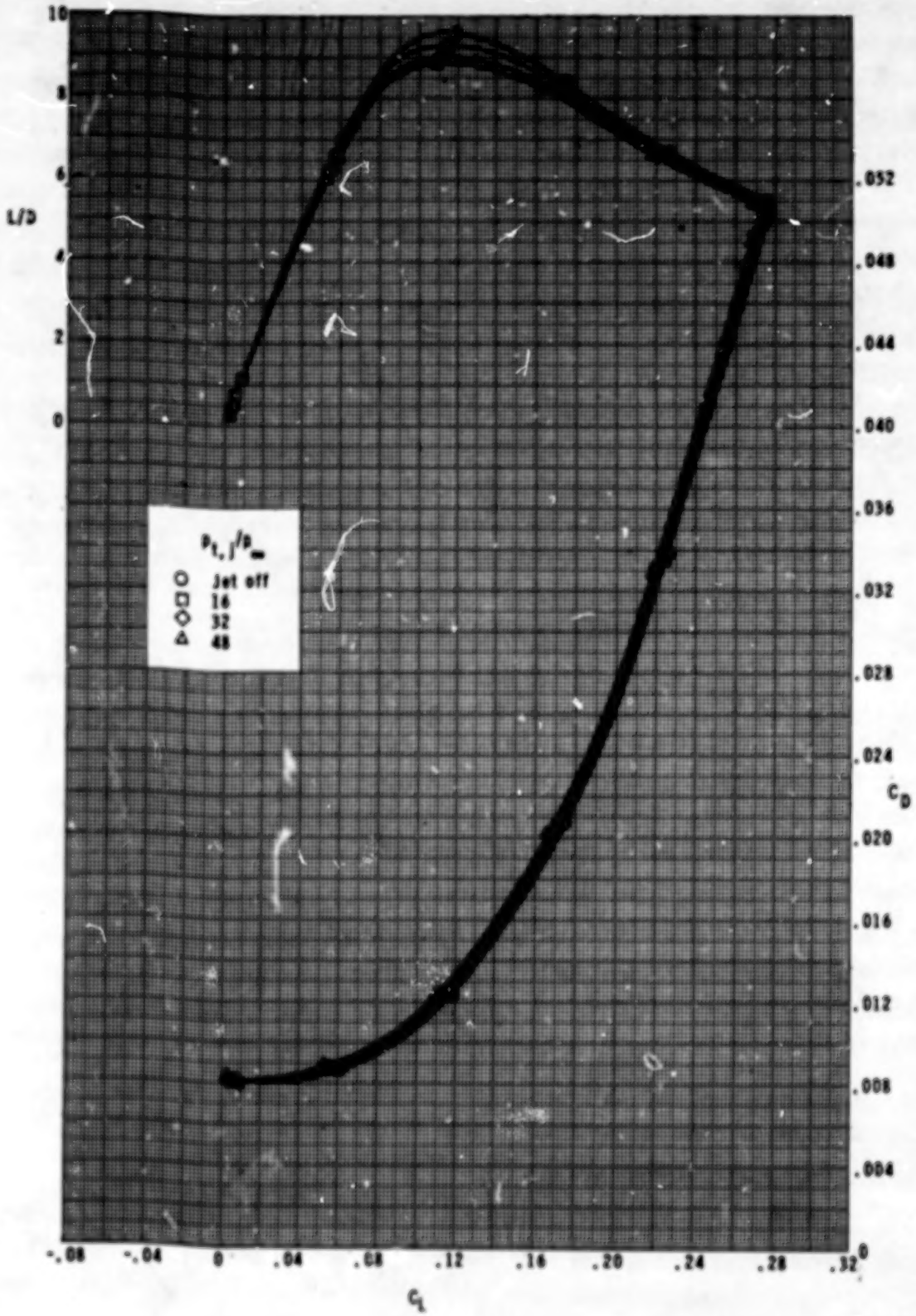

(c) Concluded.

Figure 6.- Concluded.

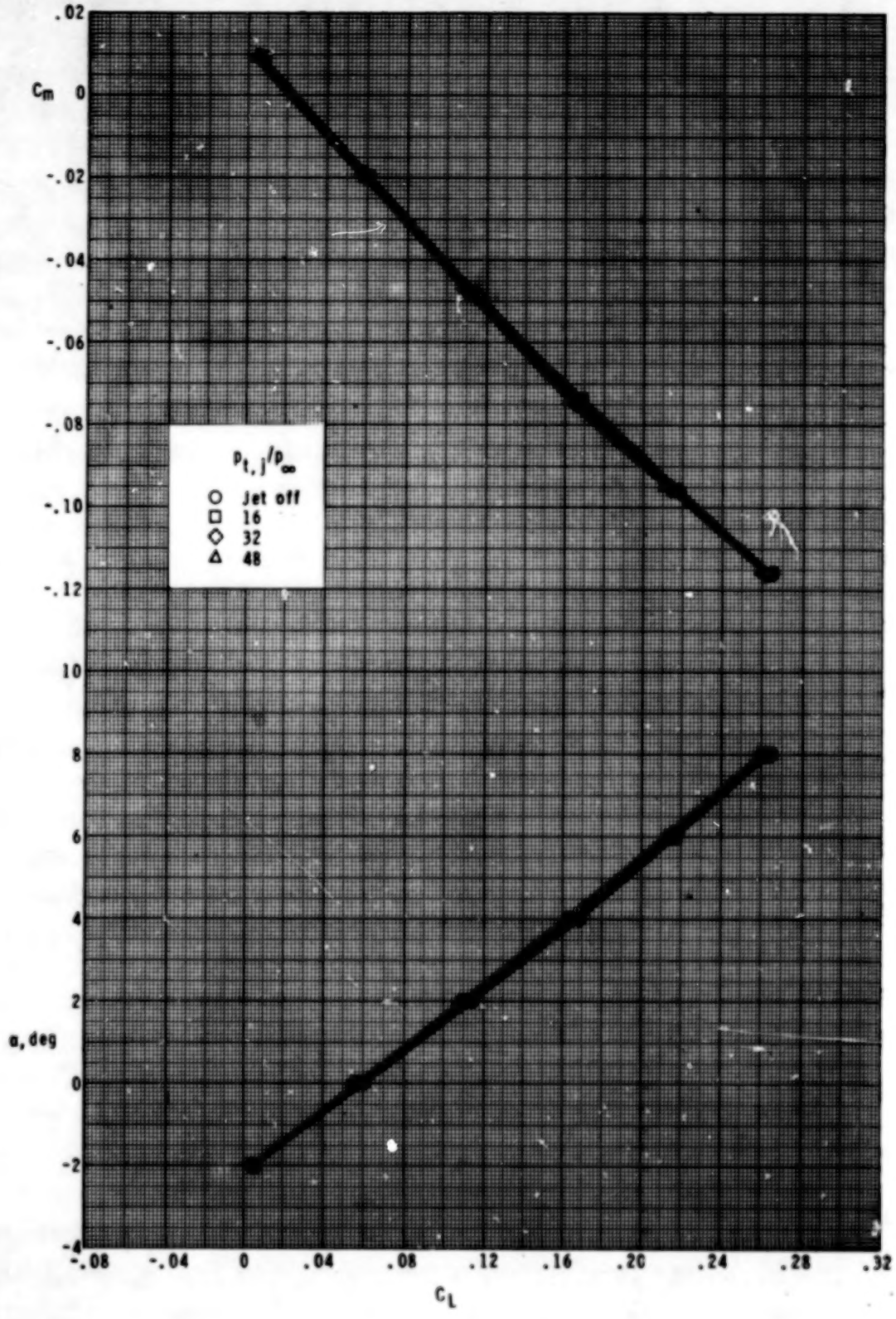

(a) Primary nozzle.

Figure 7.- Effect of helium jet flow on longitudinal aerodynamic characteristics of wing. Lower nacelle position.

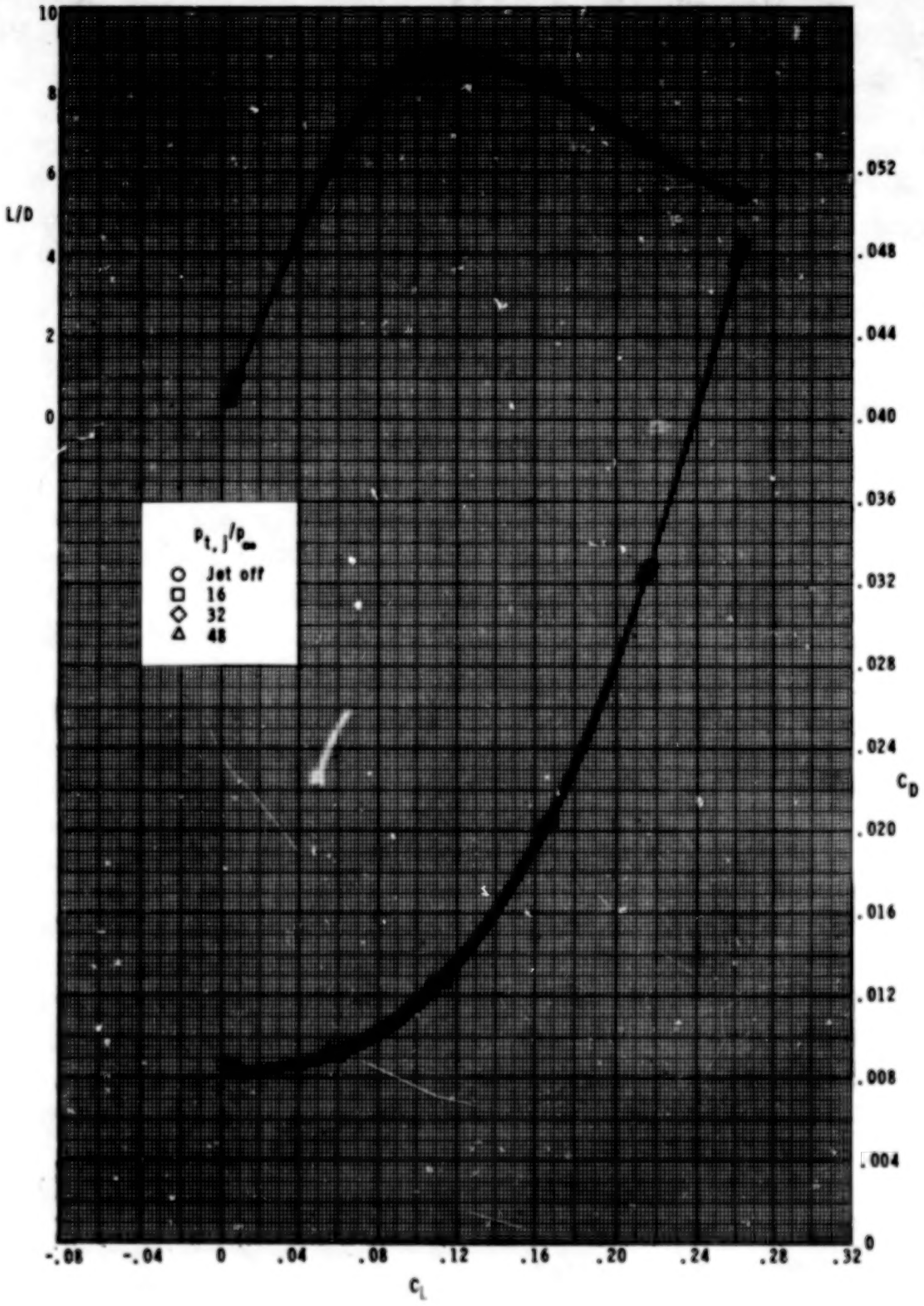

(a) Concluded.

Figure 7.- Continued.

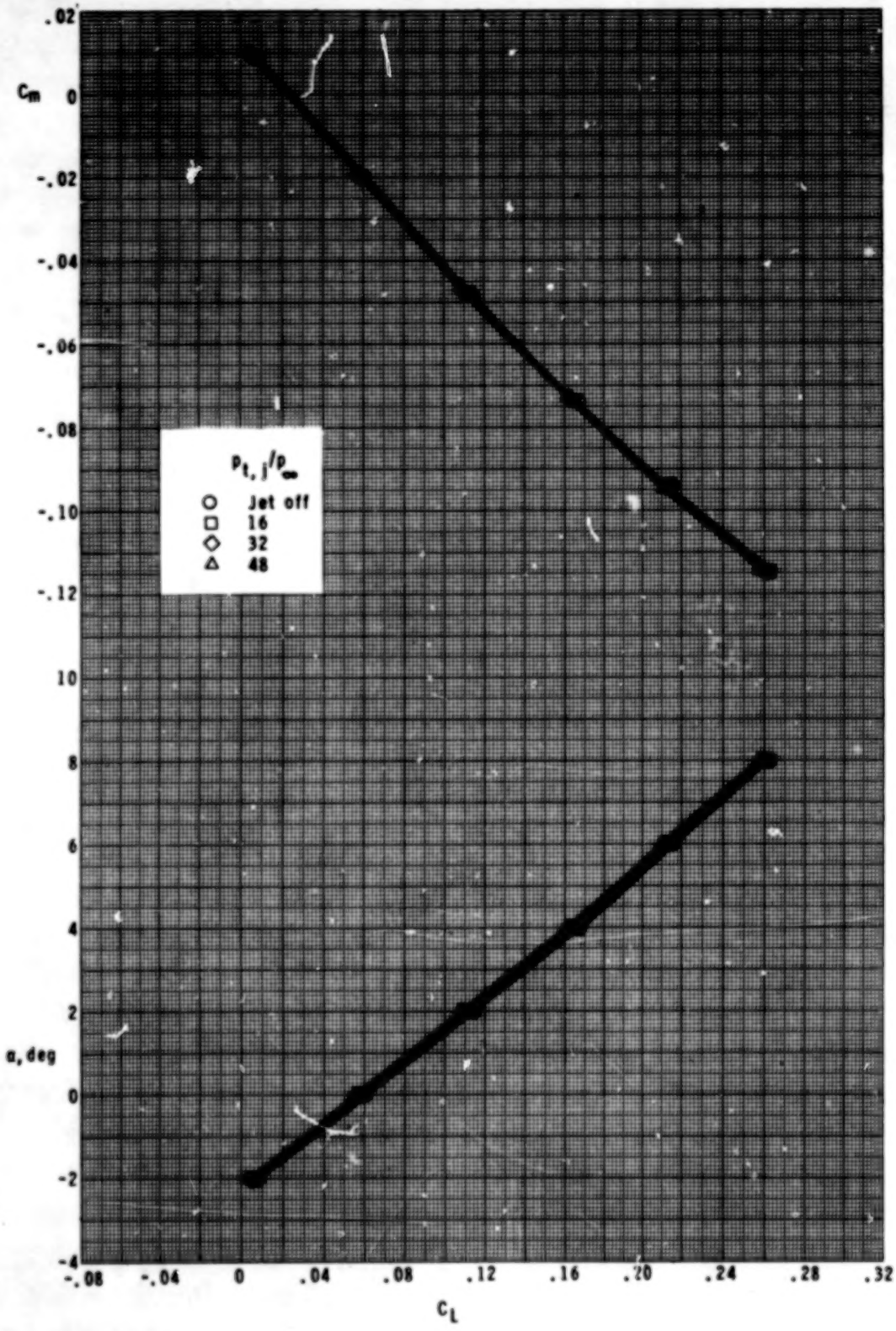

(b) Extended nozzle.

Figure 7.- Continued.

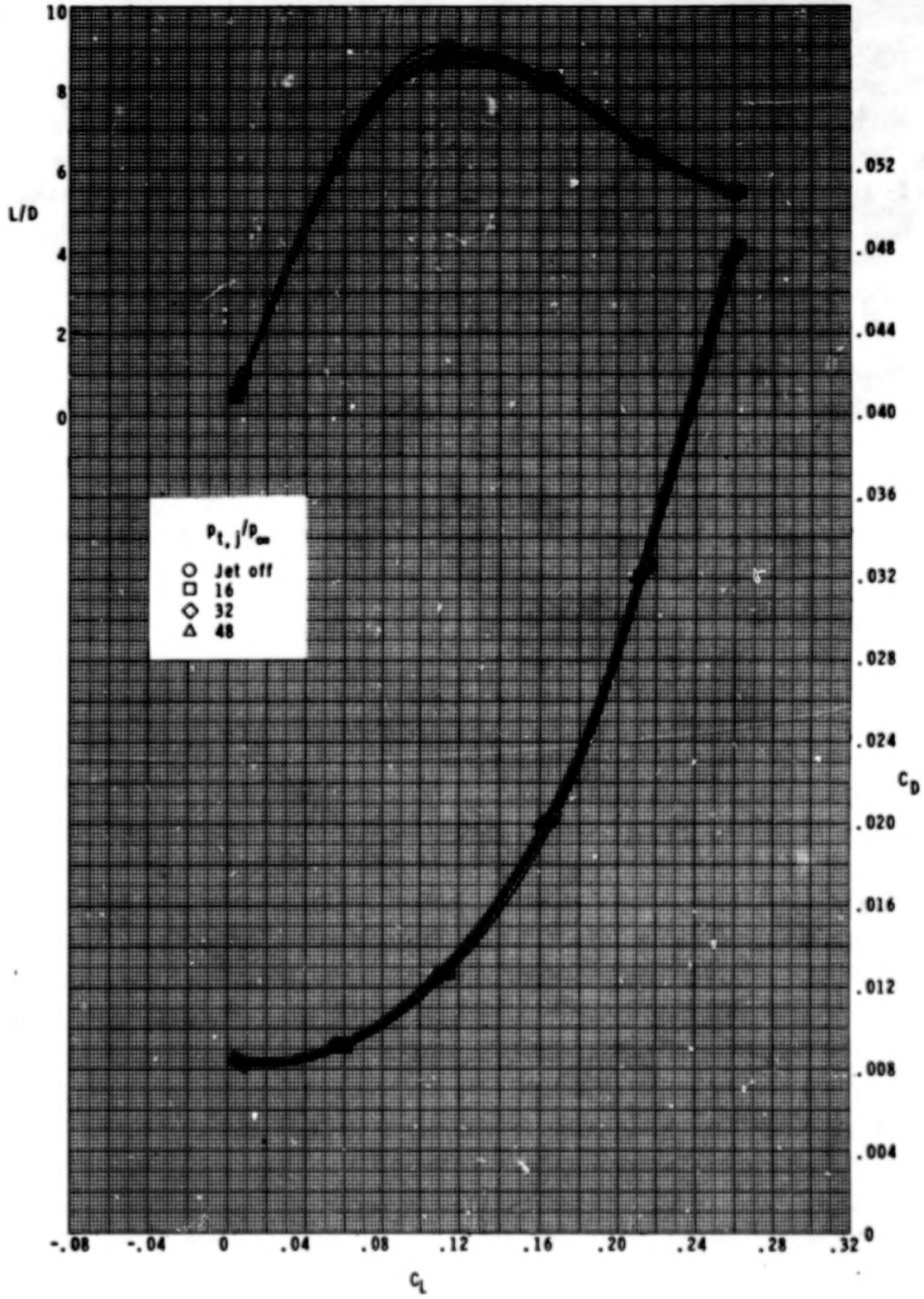

(b) Concluded.

Figure 7.- Continued.

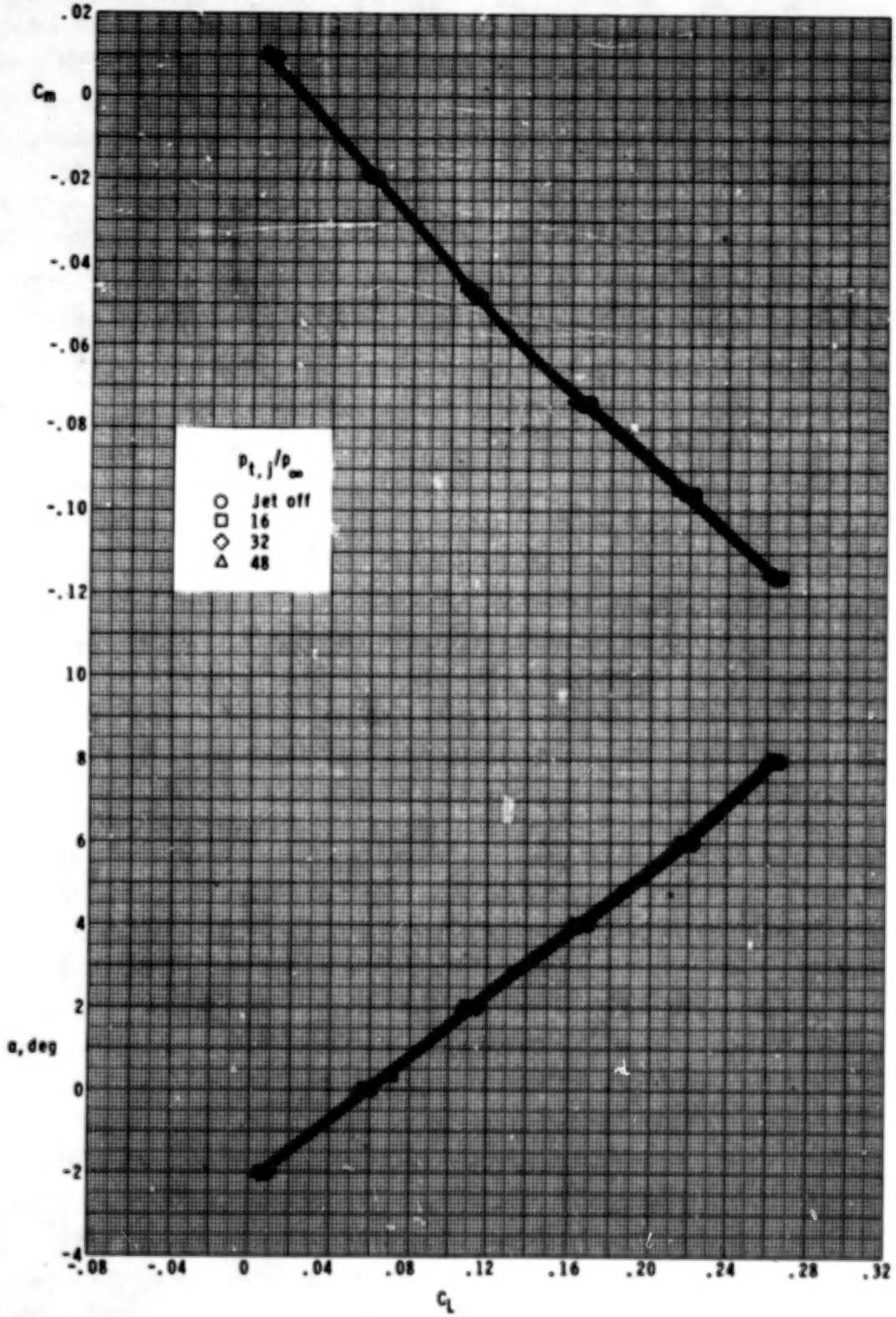

(c) Canted nozzle.

Figure 7.- Continued.

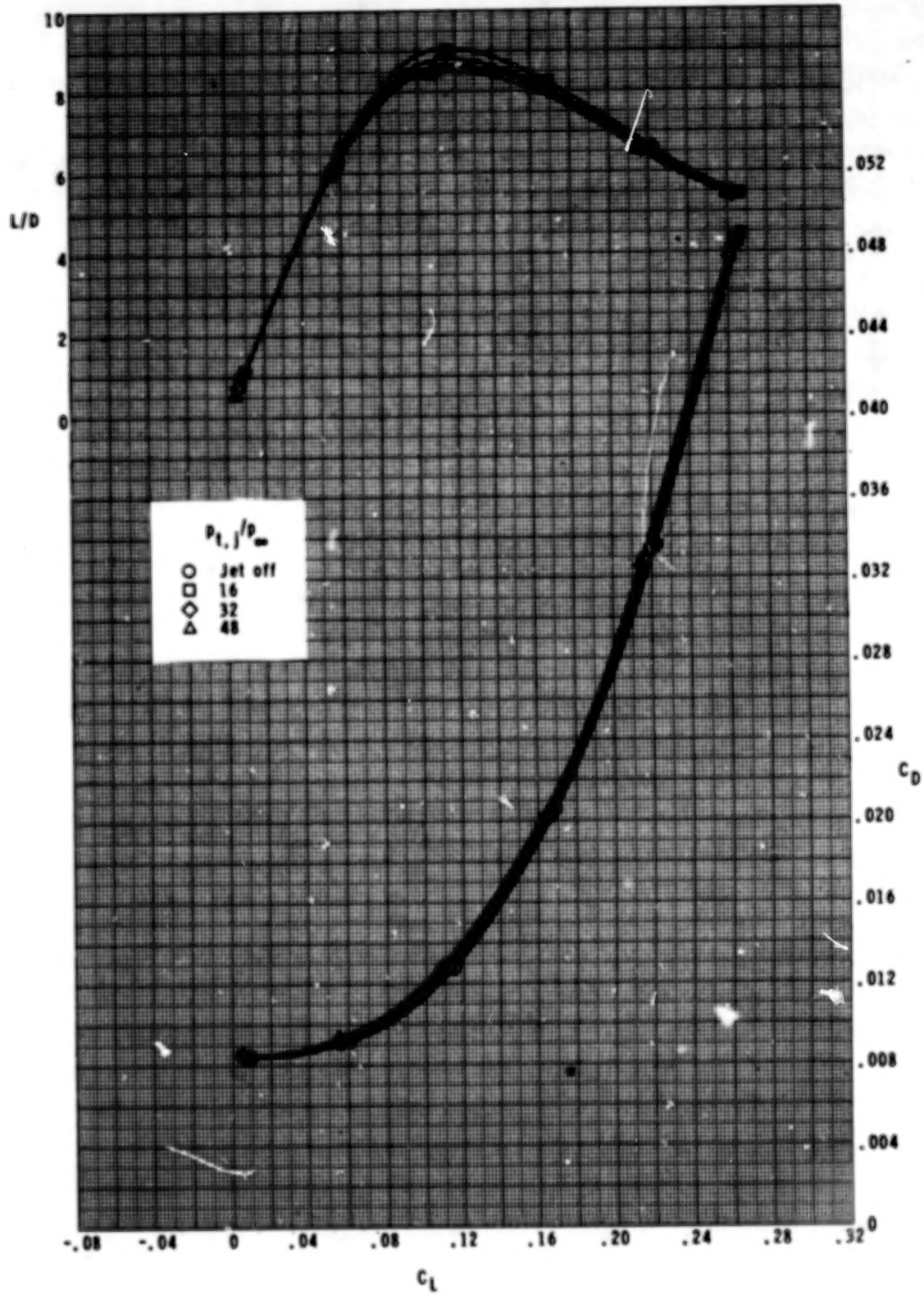

(c) Concluded.

Figure 7.- Concluded.

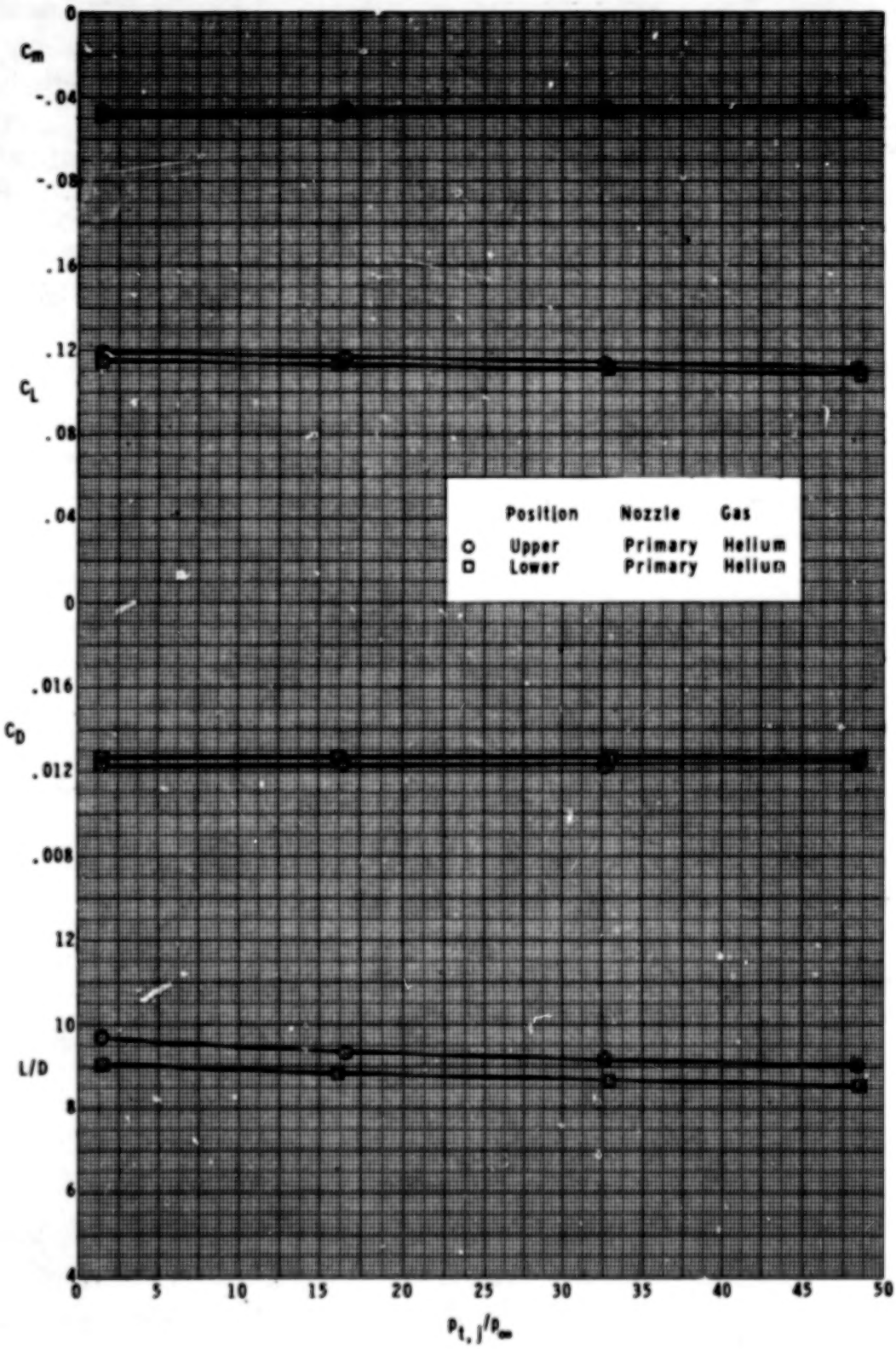

Figure 8.- Effect of vertical nacelle position and nozzle pressure ratio on longitudinal aerodynamic characteristics of wing. Helium gas; $\alpha = 2^\circ$.

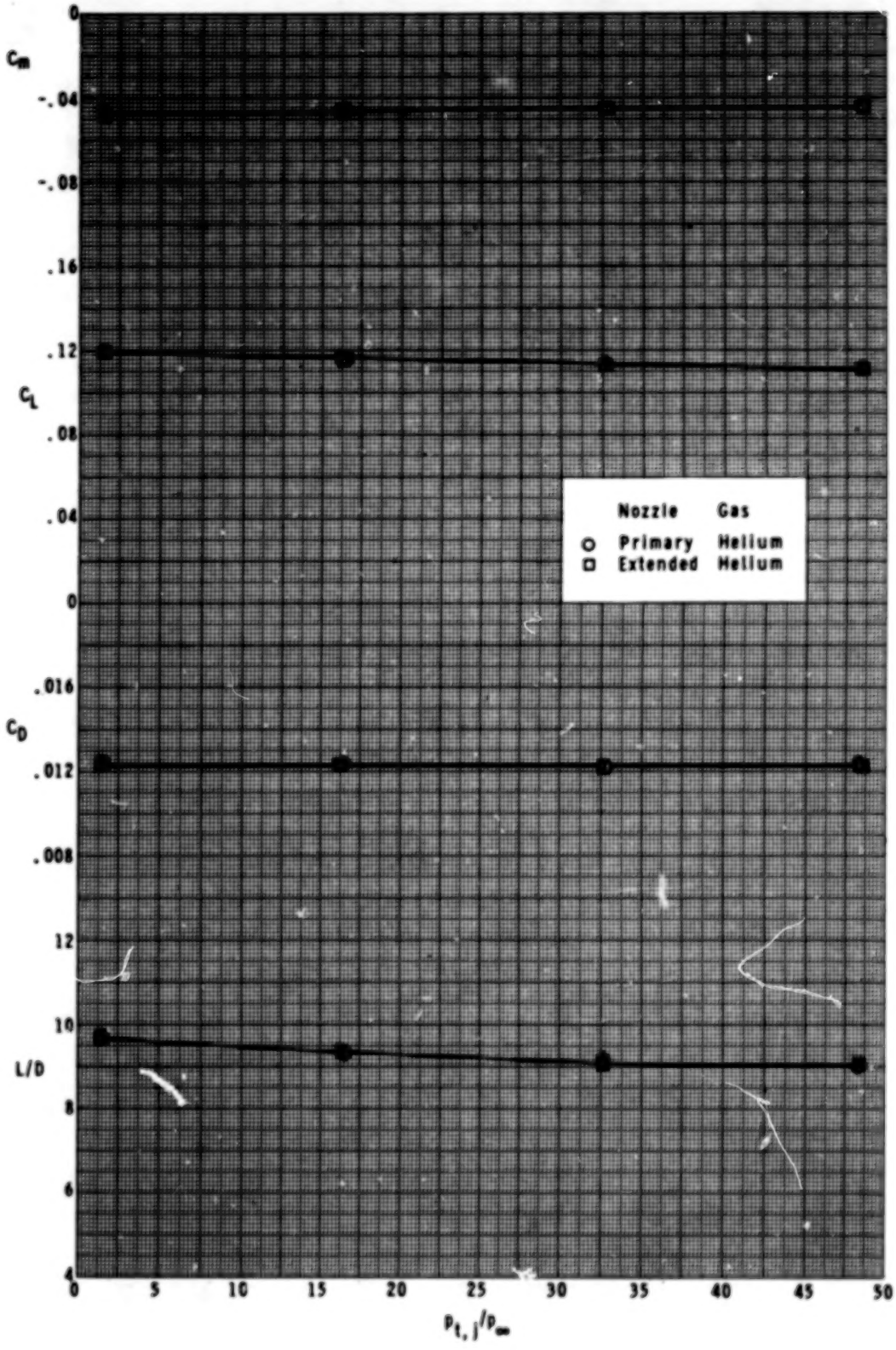

(a) Upper position.

Figure 9.- Effect of longitudinal nacelle position and nozzle pressure ratio on longitudinal aerodynamic characteristics of wing. Helium gas; $\alpha = 2^\circ$.

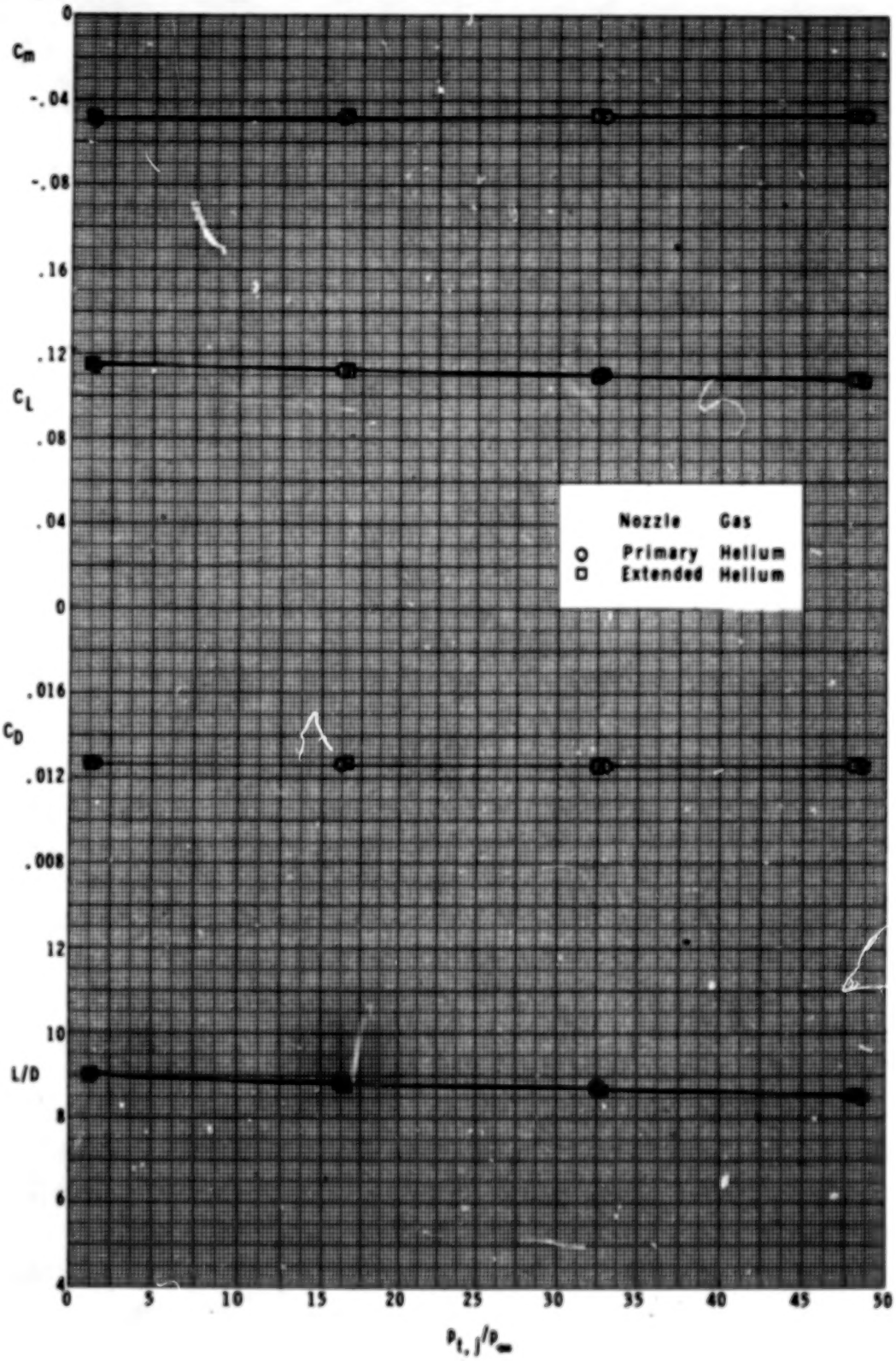

(b) Lower position.

Figure 9.- Concluded.

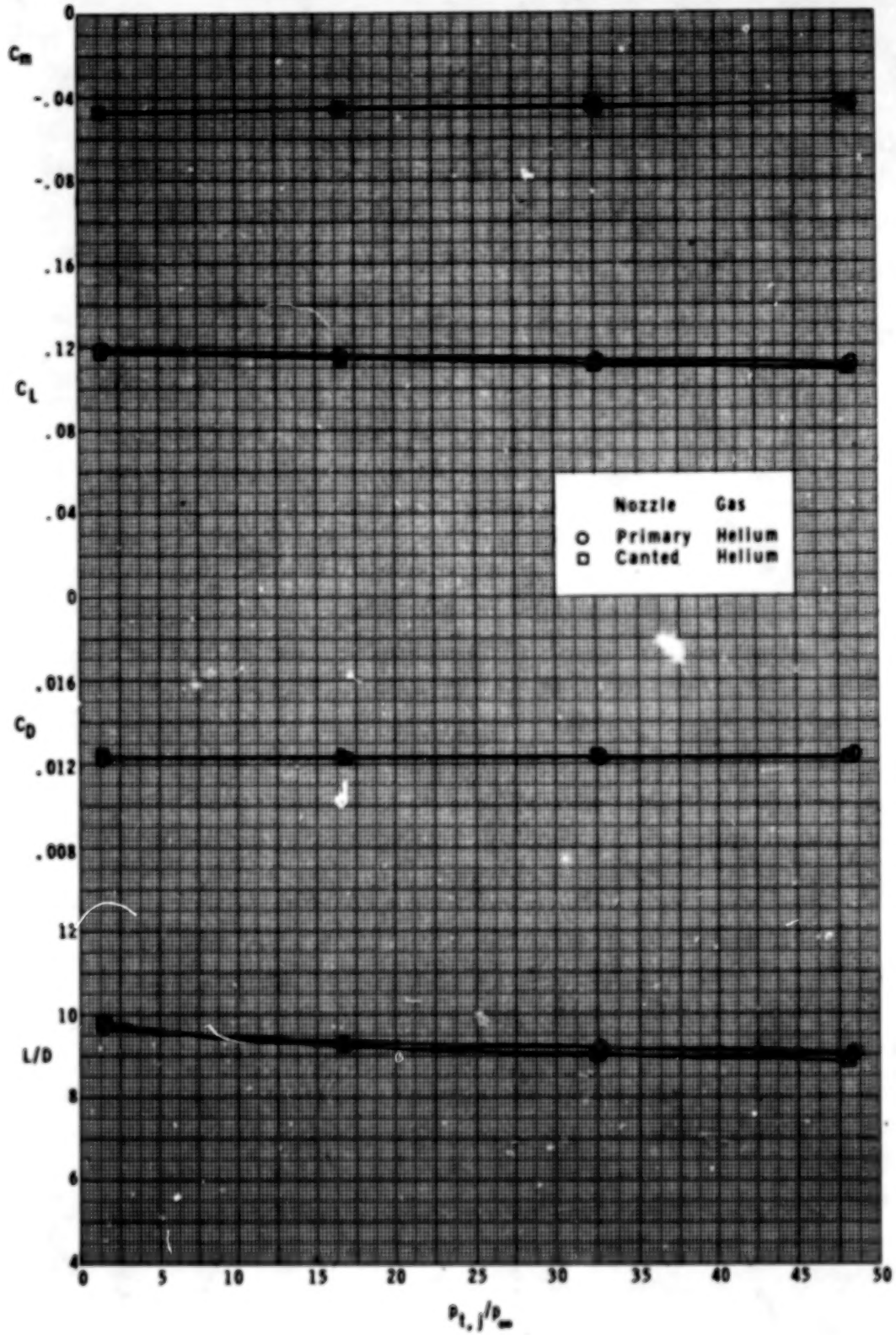

(a) Upper position.

Figure 10.- Effect of nacelle cant and nozzle pressure ratio on longitudinal aerodynamic characteristics of wing. Helium gas; $\alpha = 2^{\circ}$.

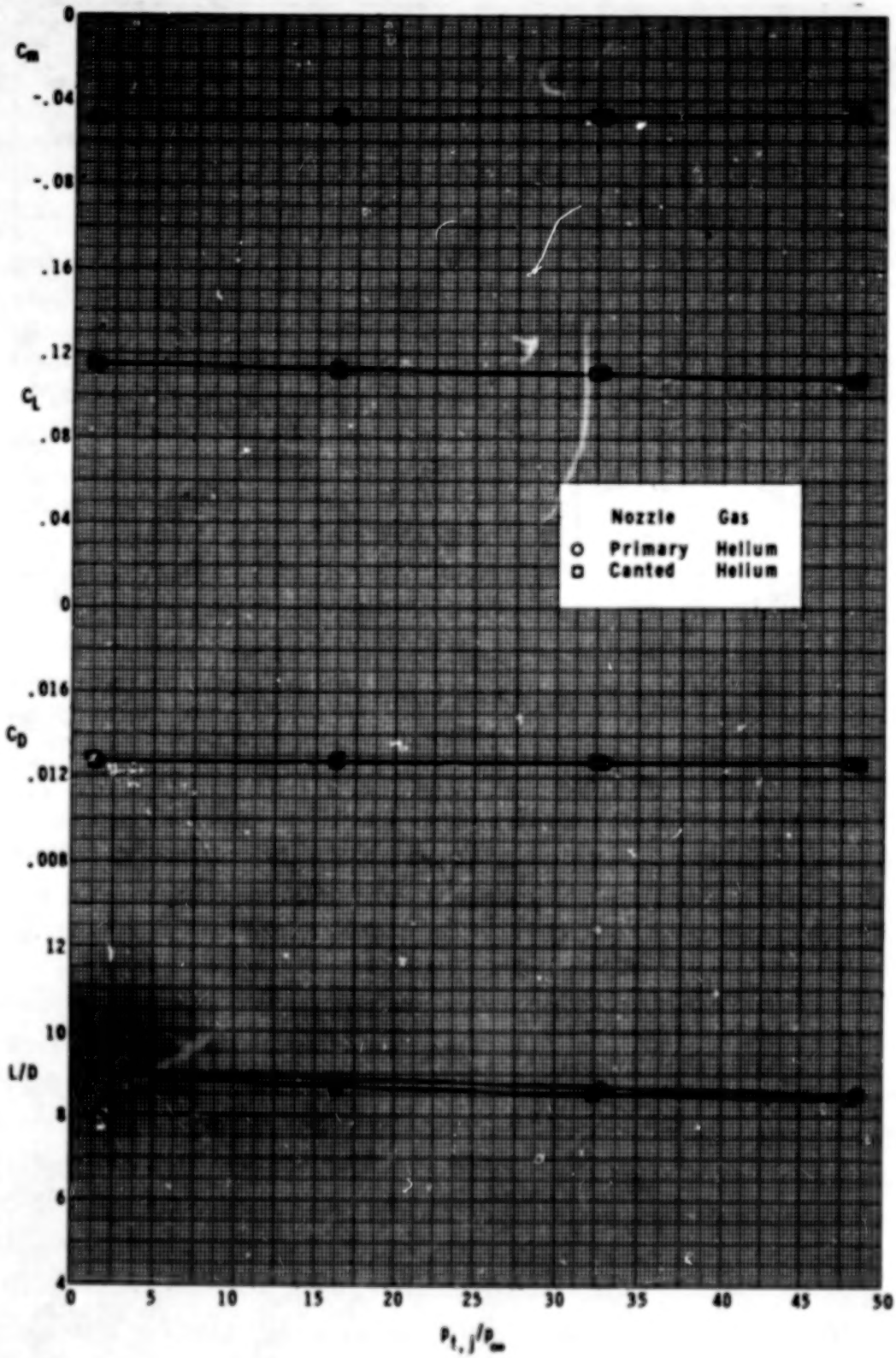

(b) Lower position.

Figure 10.- Concluded.

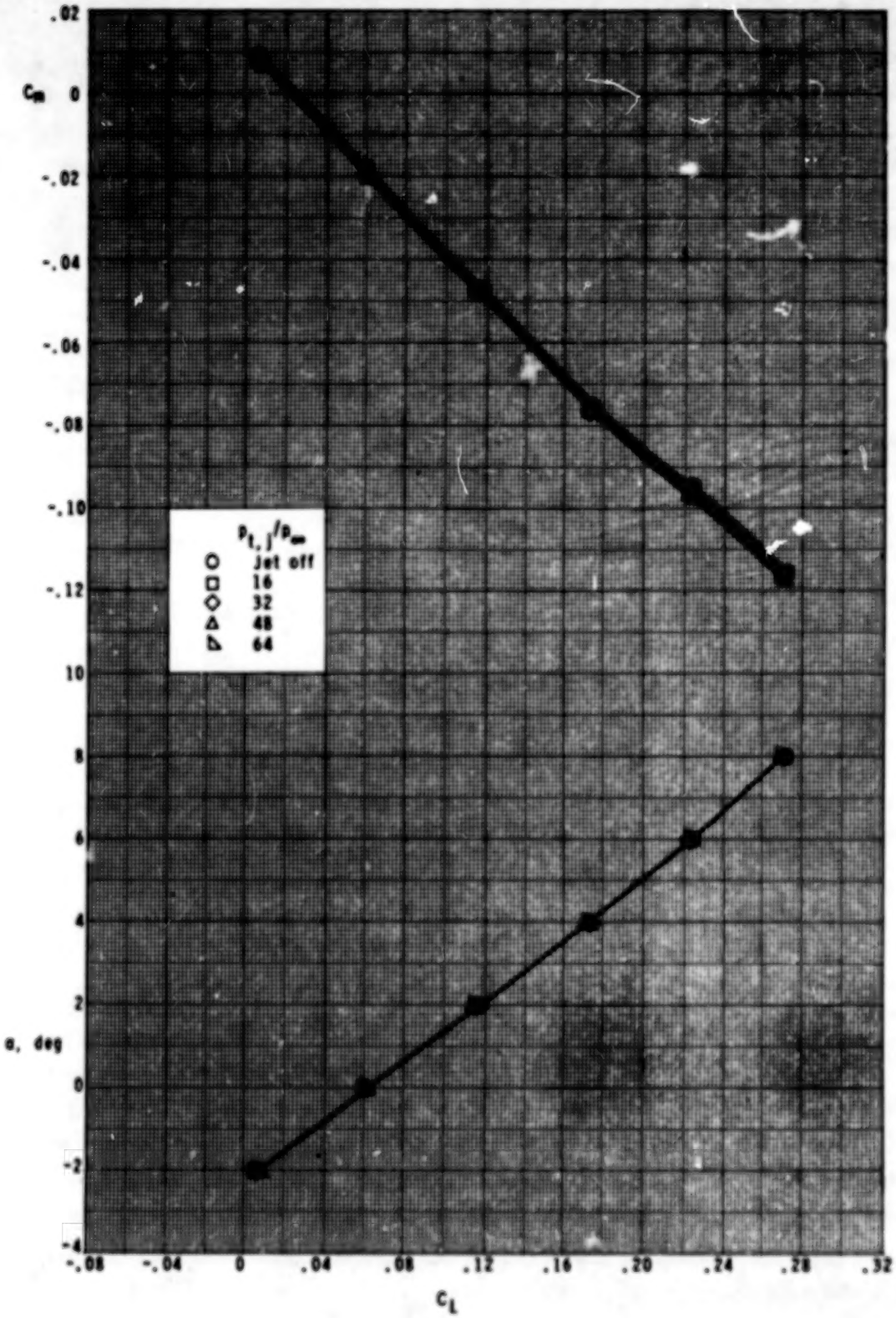

(a) Primary nozzle.

Figure 11.- Effect of air jet flow on longitudinal aerodynamic characteristics of wing. Upper nacelle position.

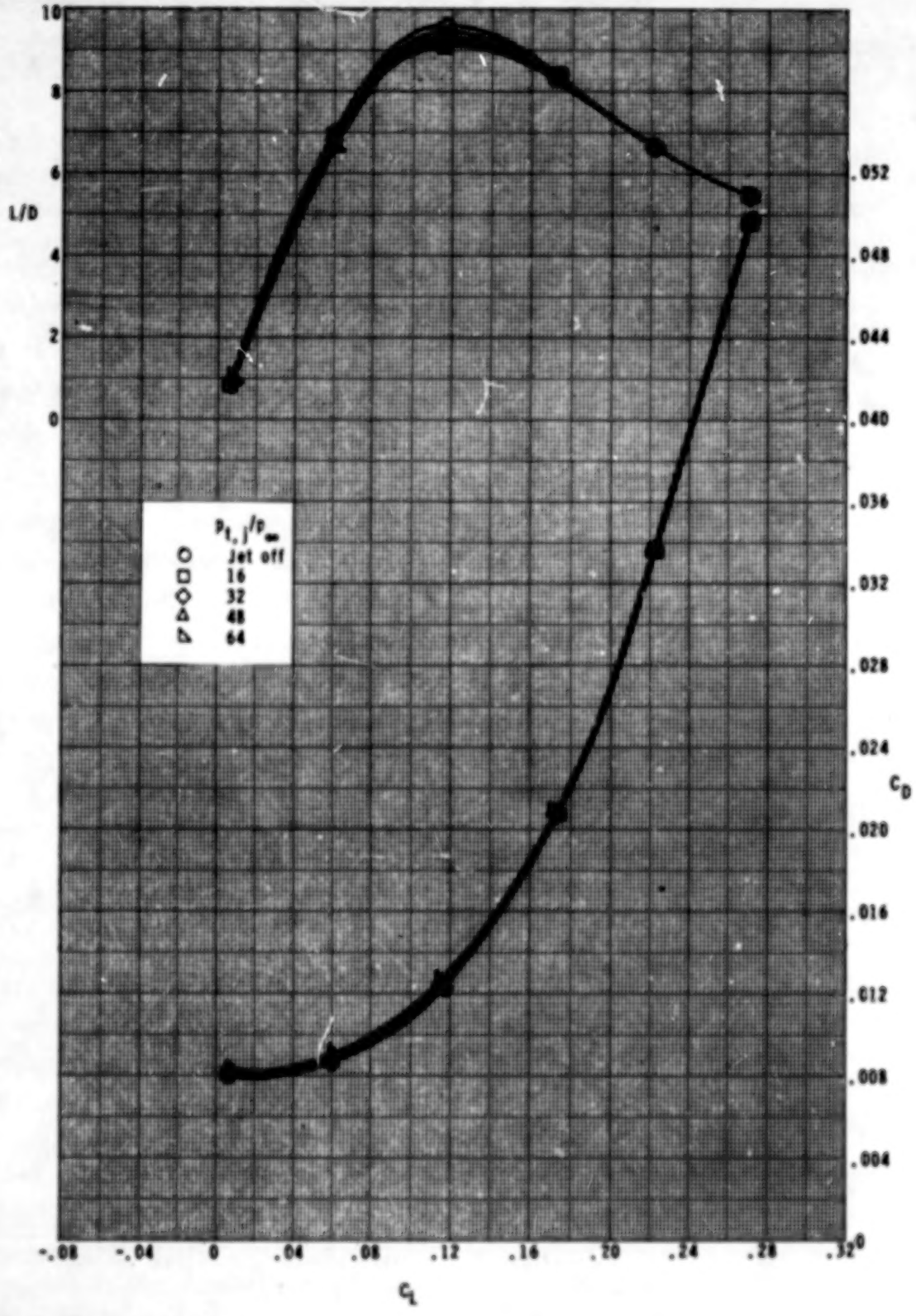

(a) Concluded.

Figure 11.- Continued.

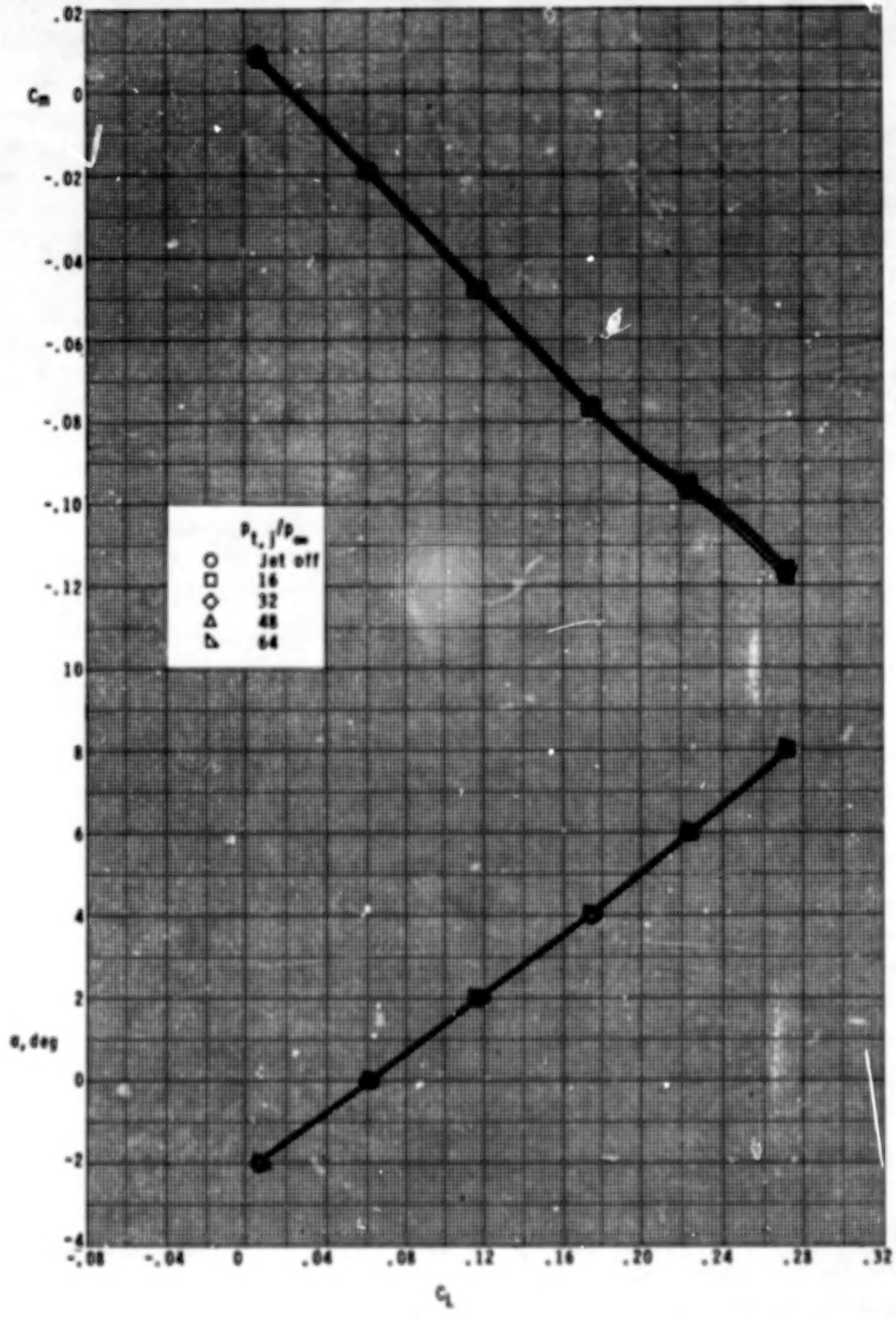

(b) Extended nozzle.

Figure 11.- Continued.

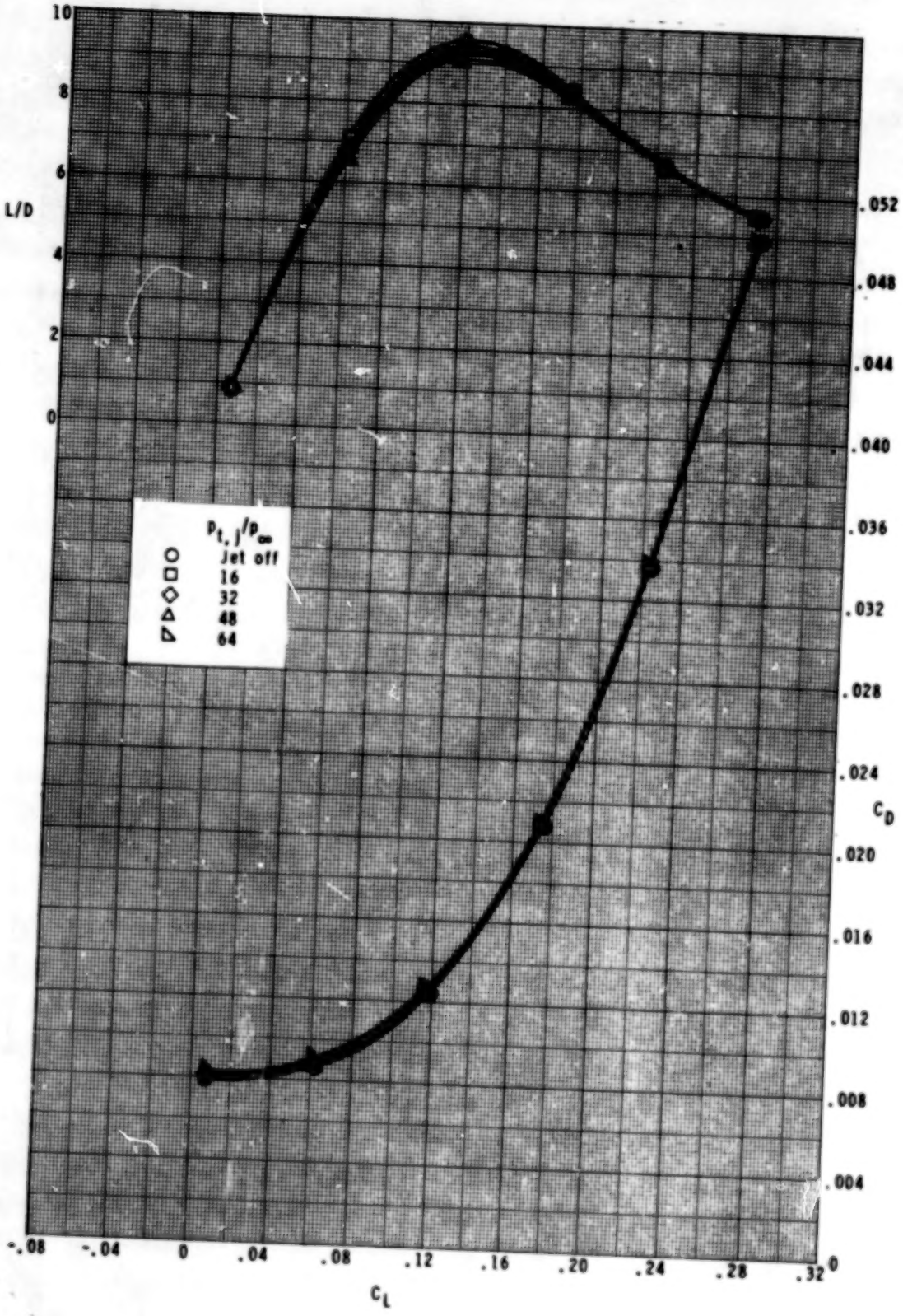

(b) Concluded.

Figure 11.- Continued.

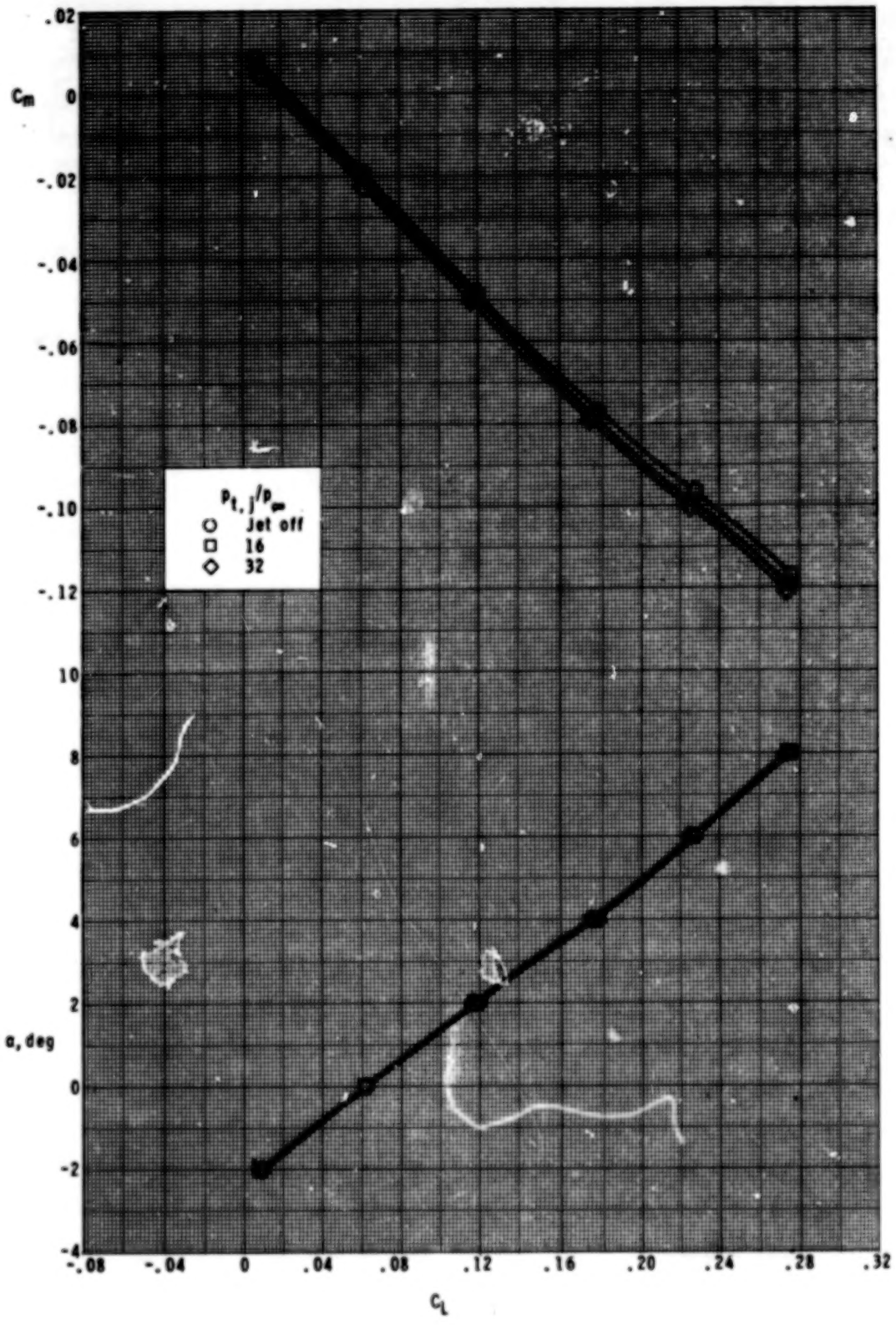

(c) Air nozzle.

Figure 11.- Continued.

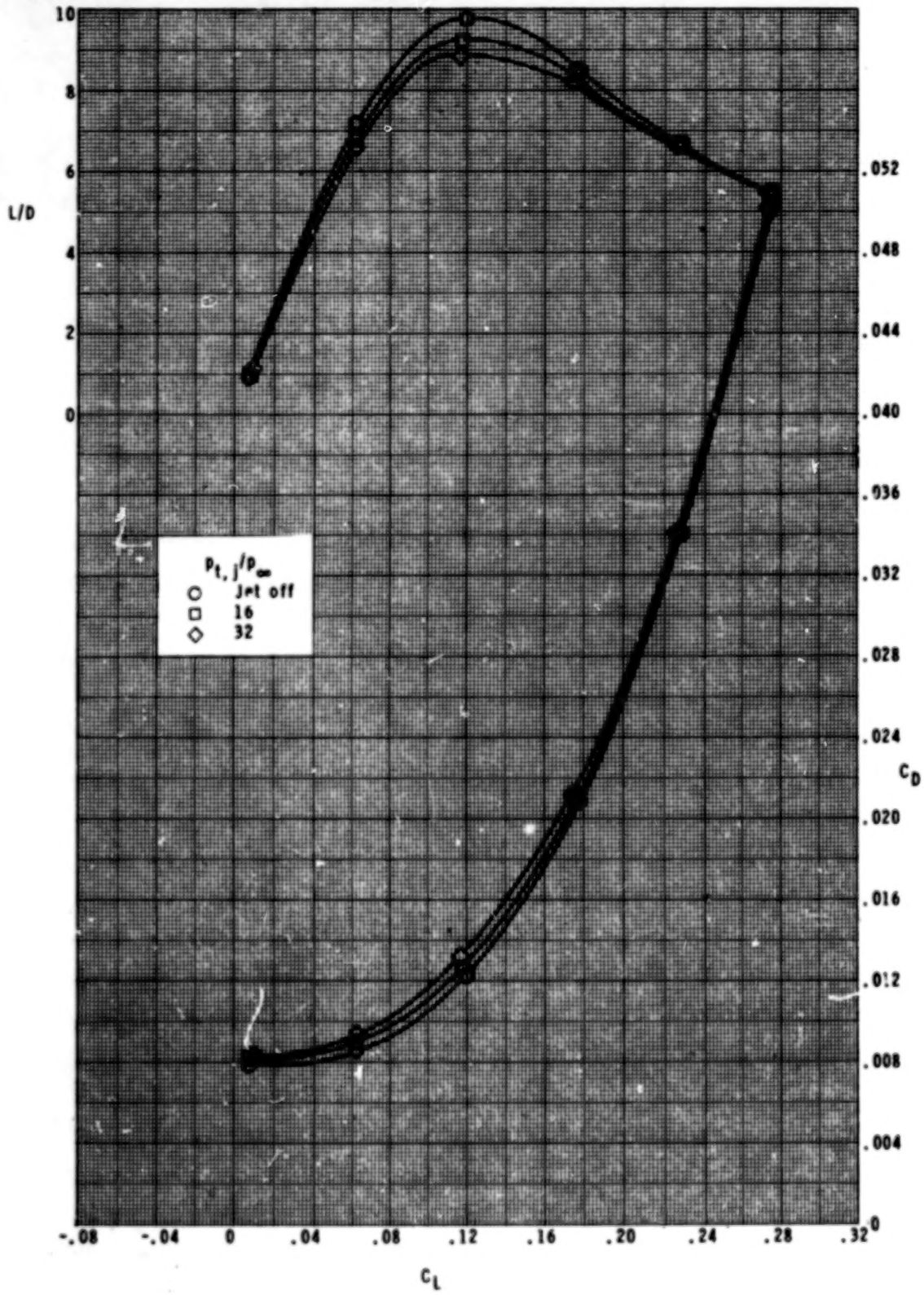

(c) Concluded.

Figure 11.- Concluded.

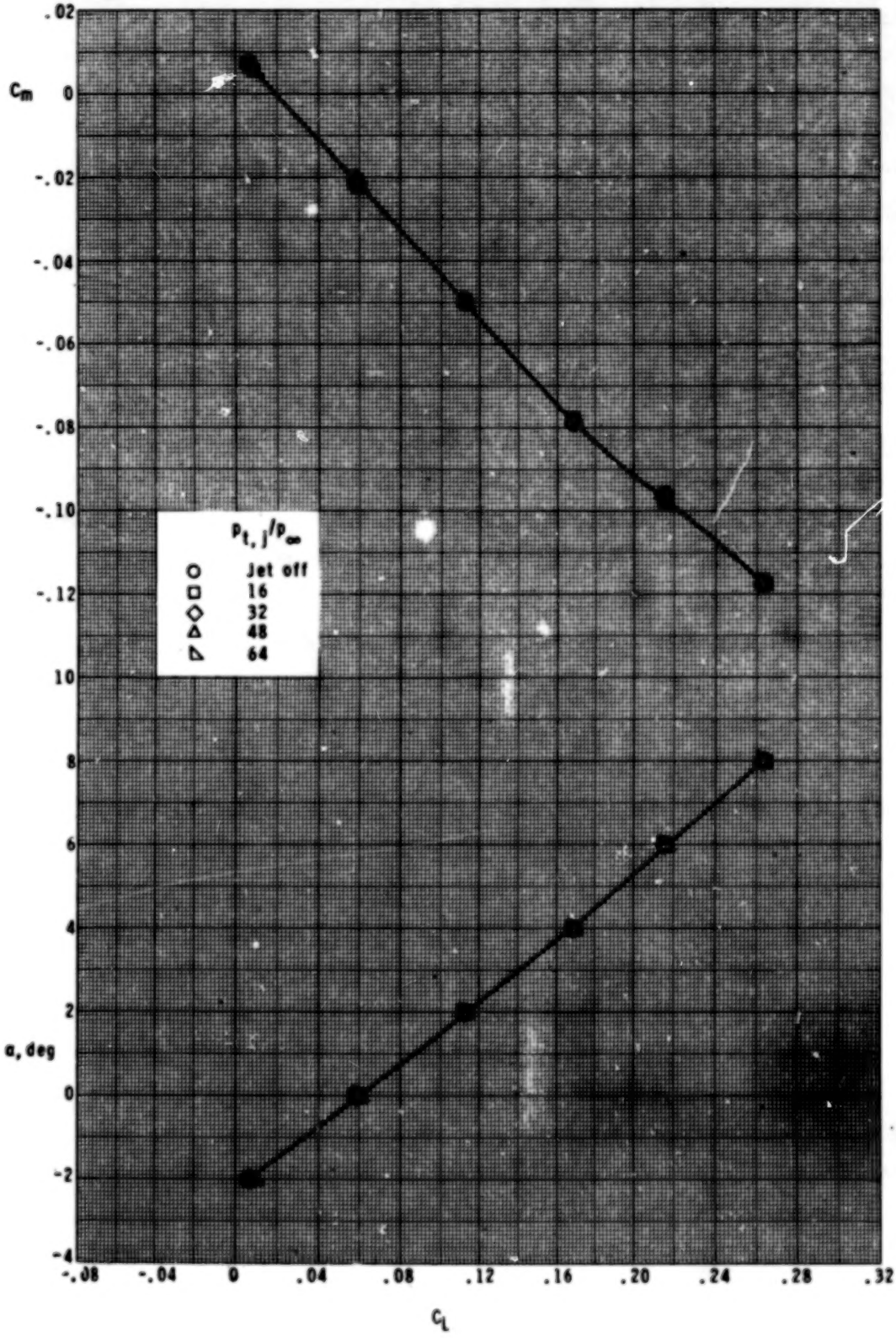

(a) Primary nozzle.

Figure 12.- Effect of air jet flow on longitudinal aerodynamic characteristics of wing. Lower nacelle position.

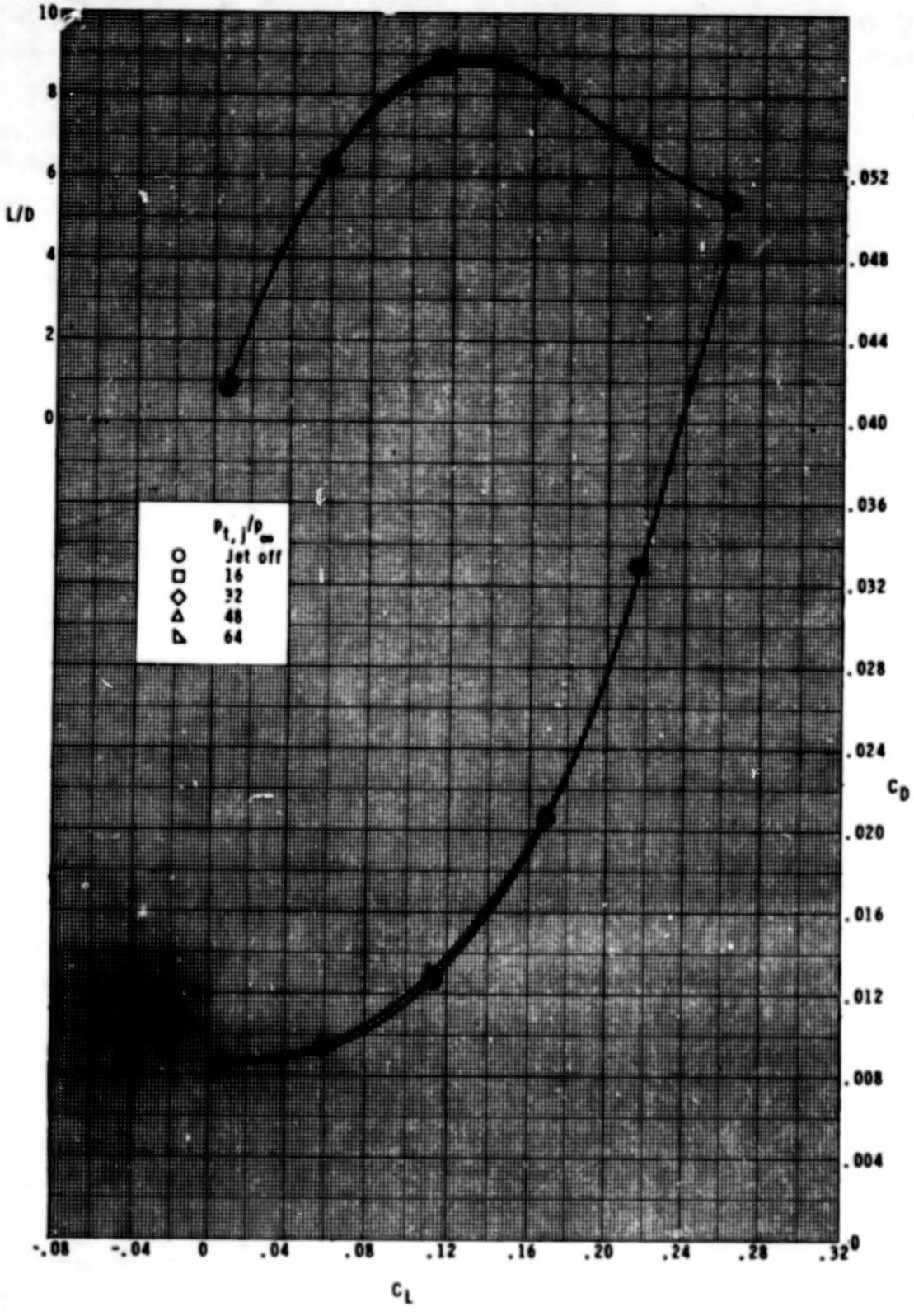

(a) Concluded.

Figure 12.- Continued.

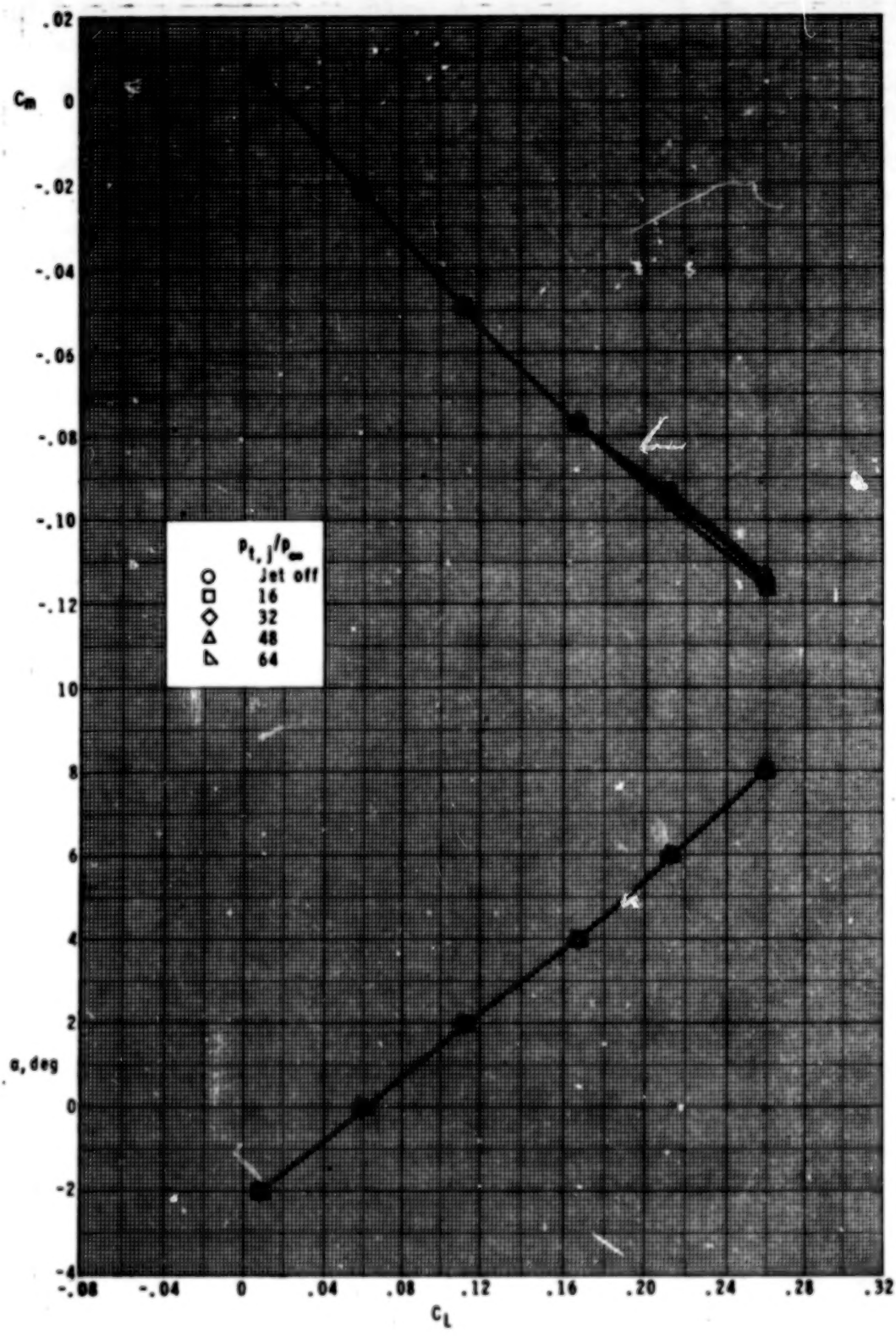

(b) Extended nozzle.

Figure 12.- Continued.

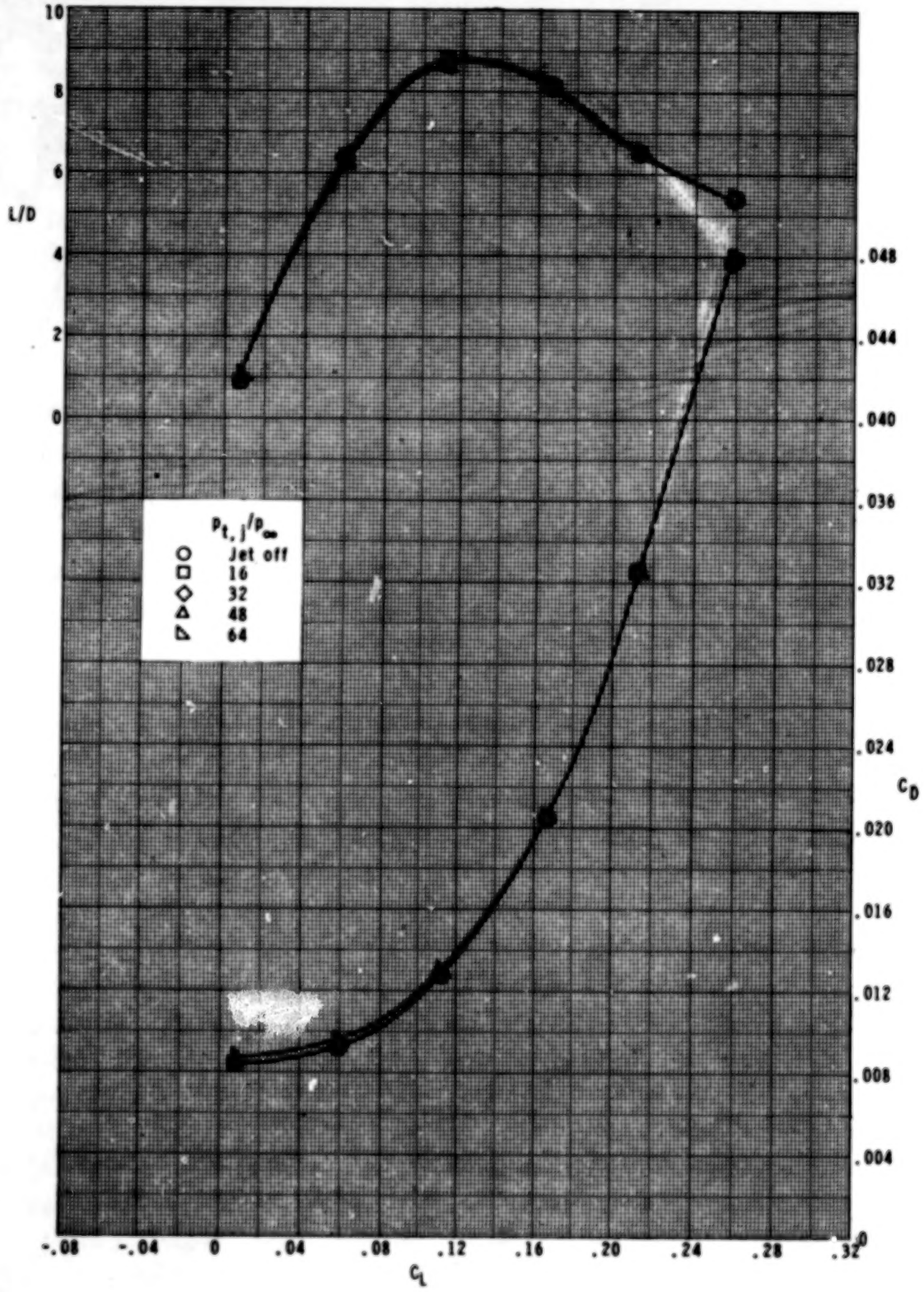

(b) Concluded.

Figure 12.- Continued.

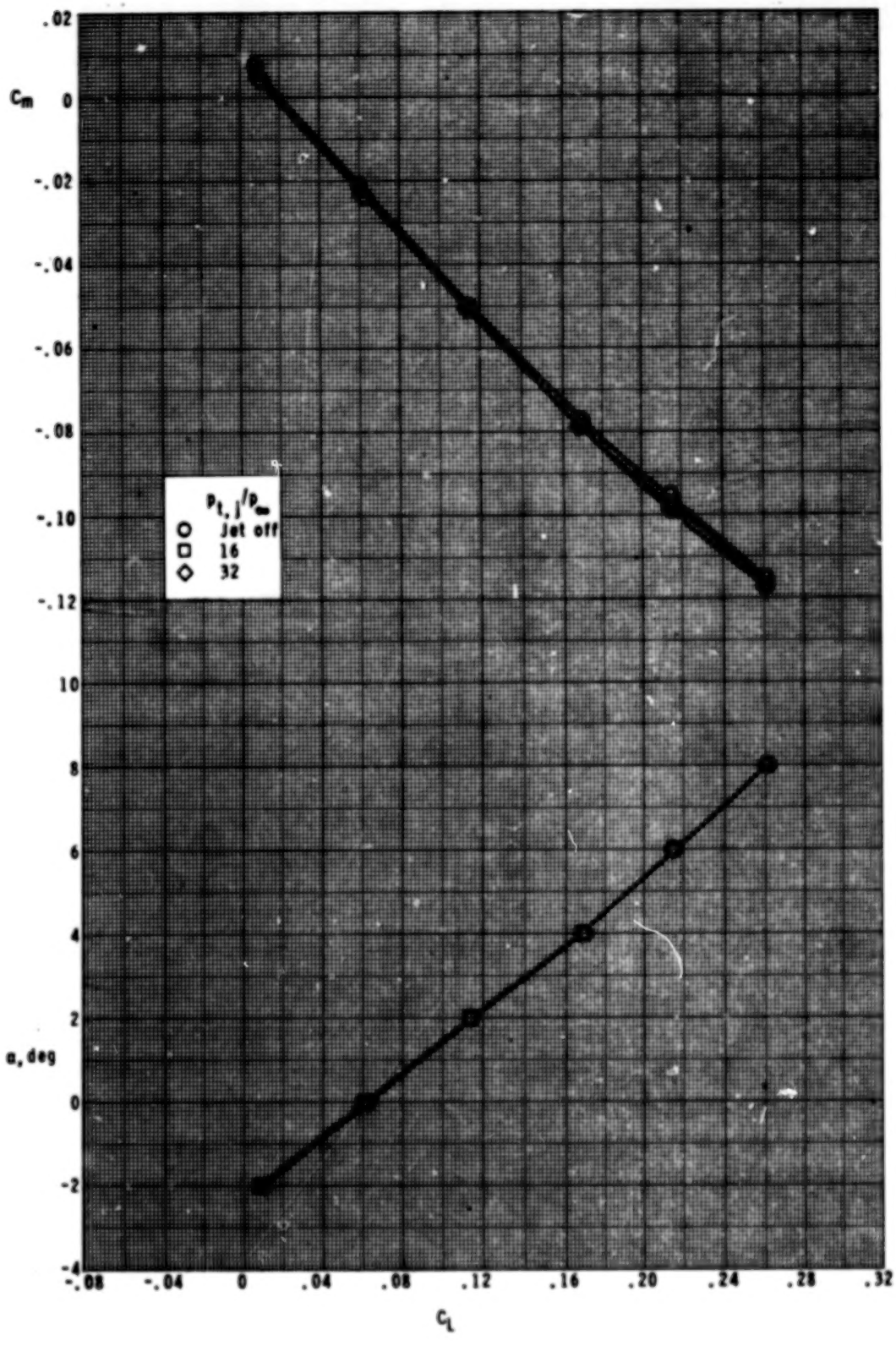

(c) Air nozzles.

Figure 12.- Continued.

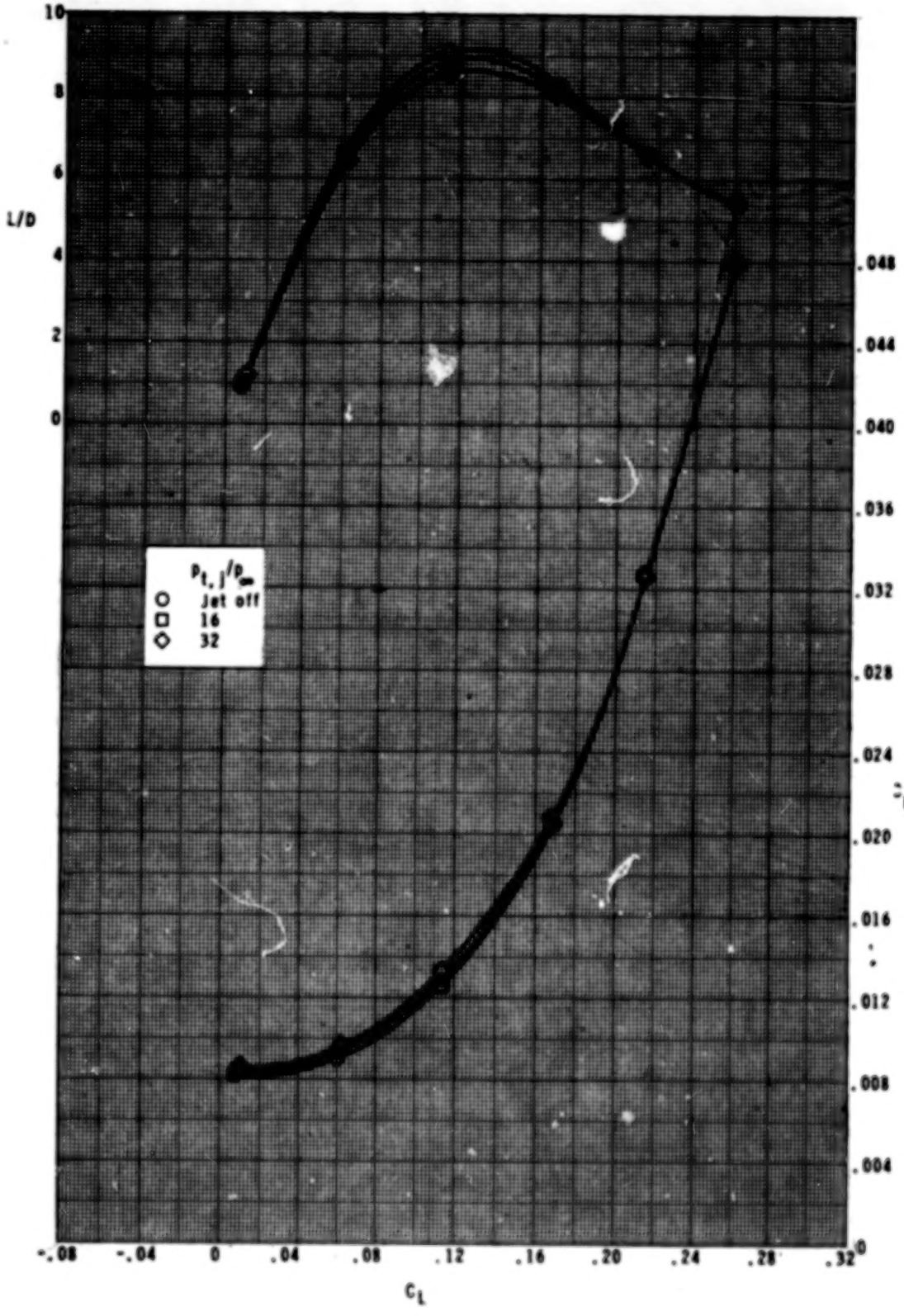

(c) Concluded.

Figure 12.- Concluded.

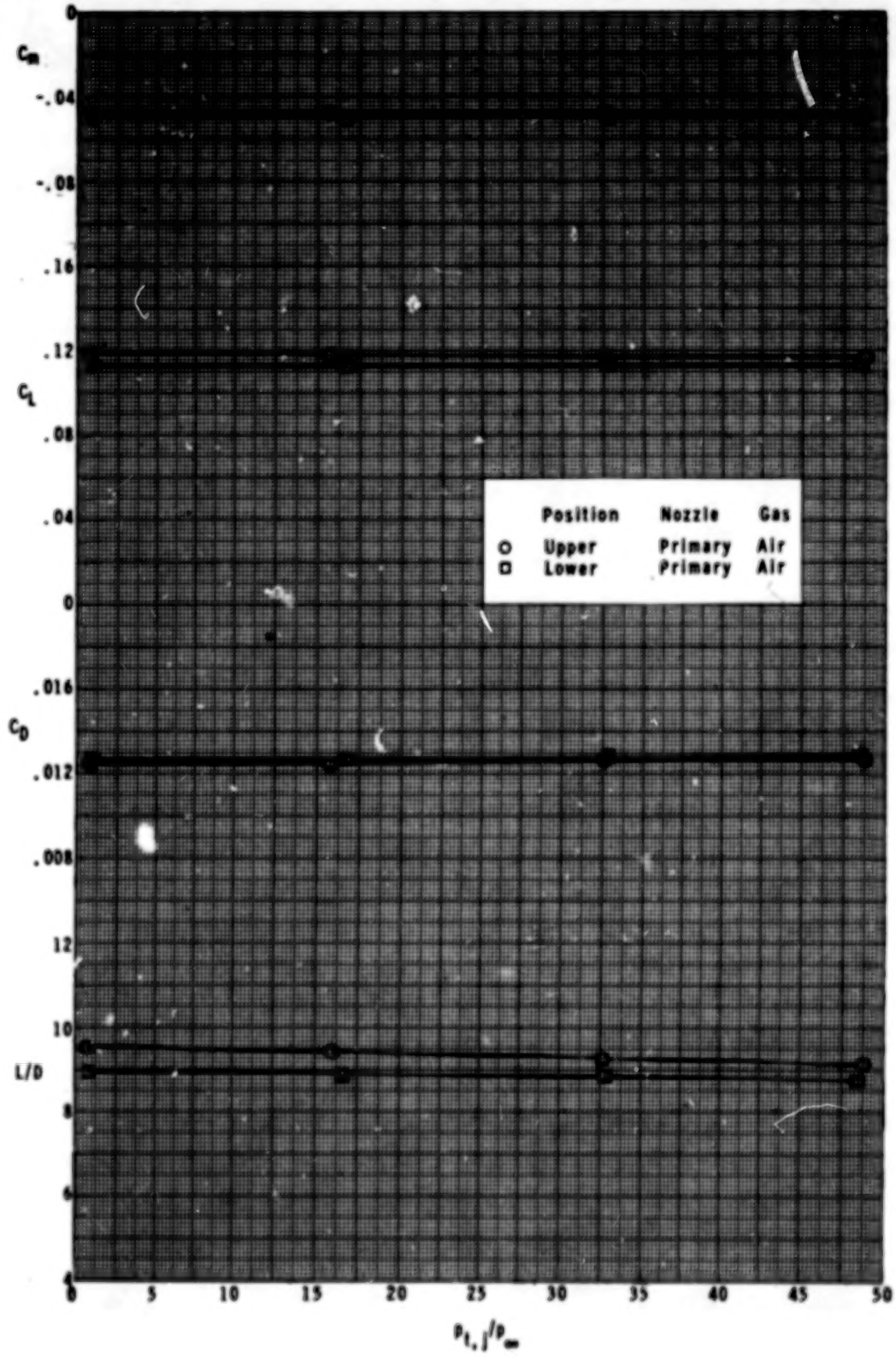

(a) Primary nozzle.

Figure 13.- Effect of vertical nacelle position and nozzle pressure ratio on longitudinal aerodynamic characteristics of wing. Air gas; $\alpha = 2^\circ$.

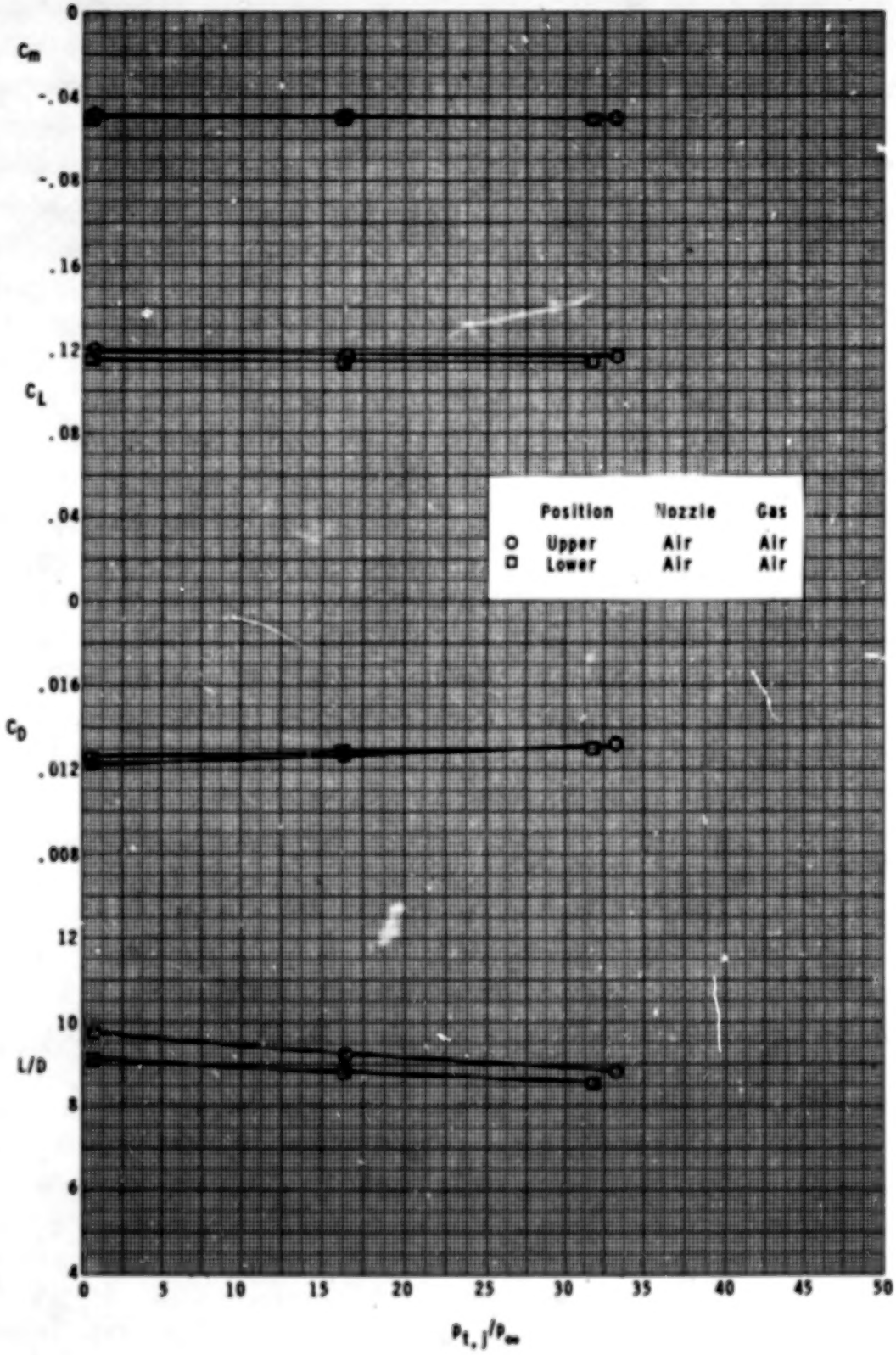

(b) Air nozzle.

Figure 13.- Concluded.

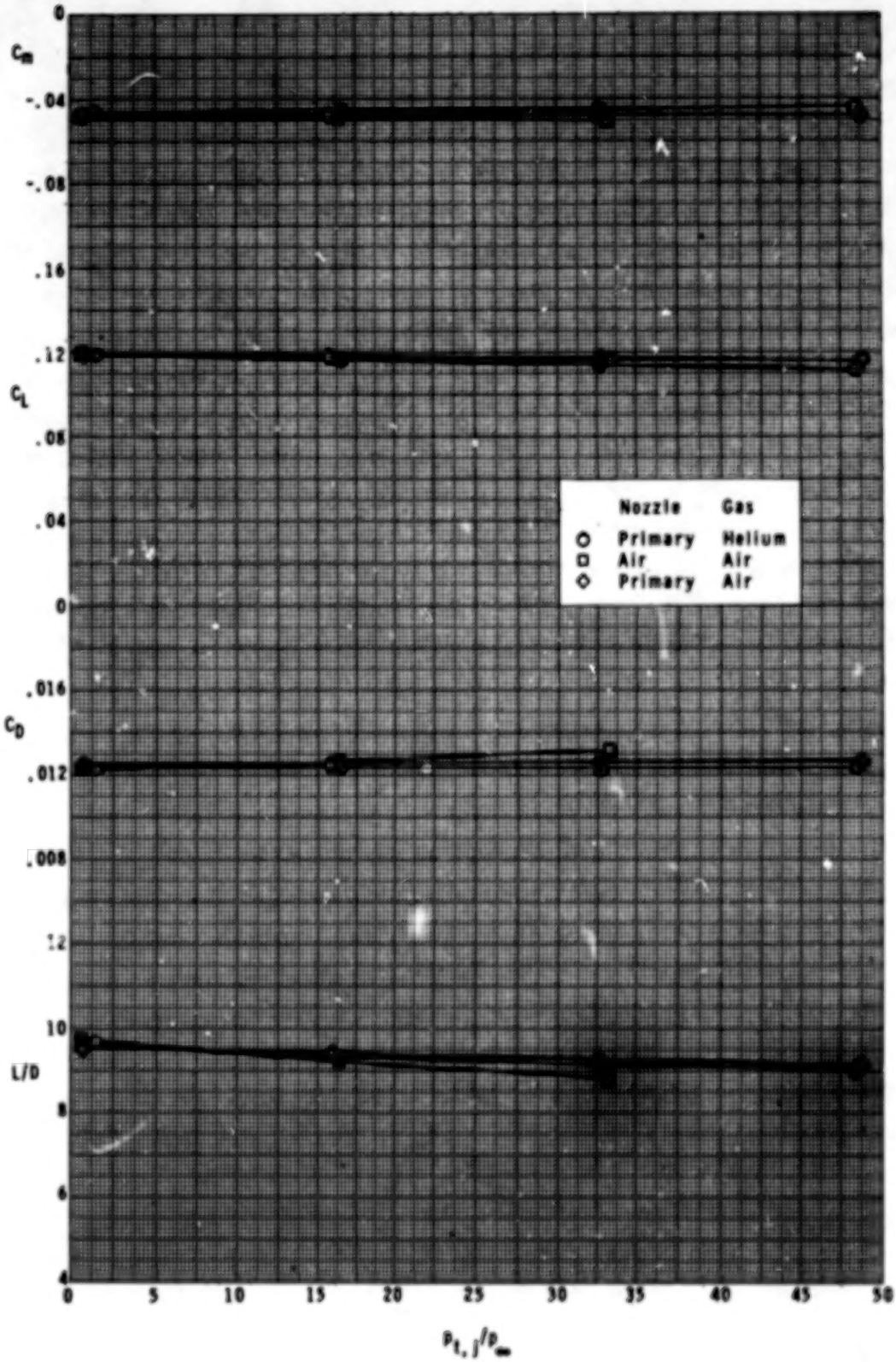

(a) Upper position.

Figure 14.- Effect of gas type and nozzle pressure ratio on longitudinal aerodynamic characteristics of wing. $\alpha = 2^{\circ}$.

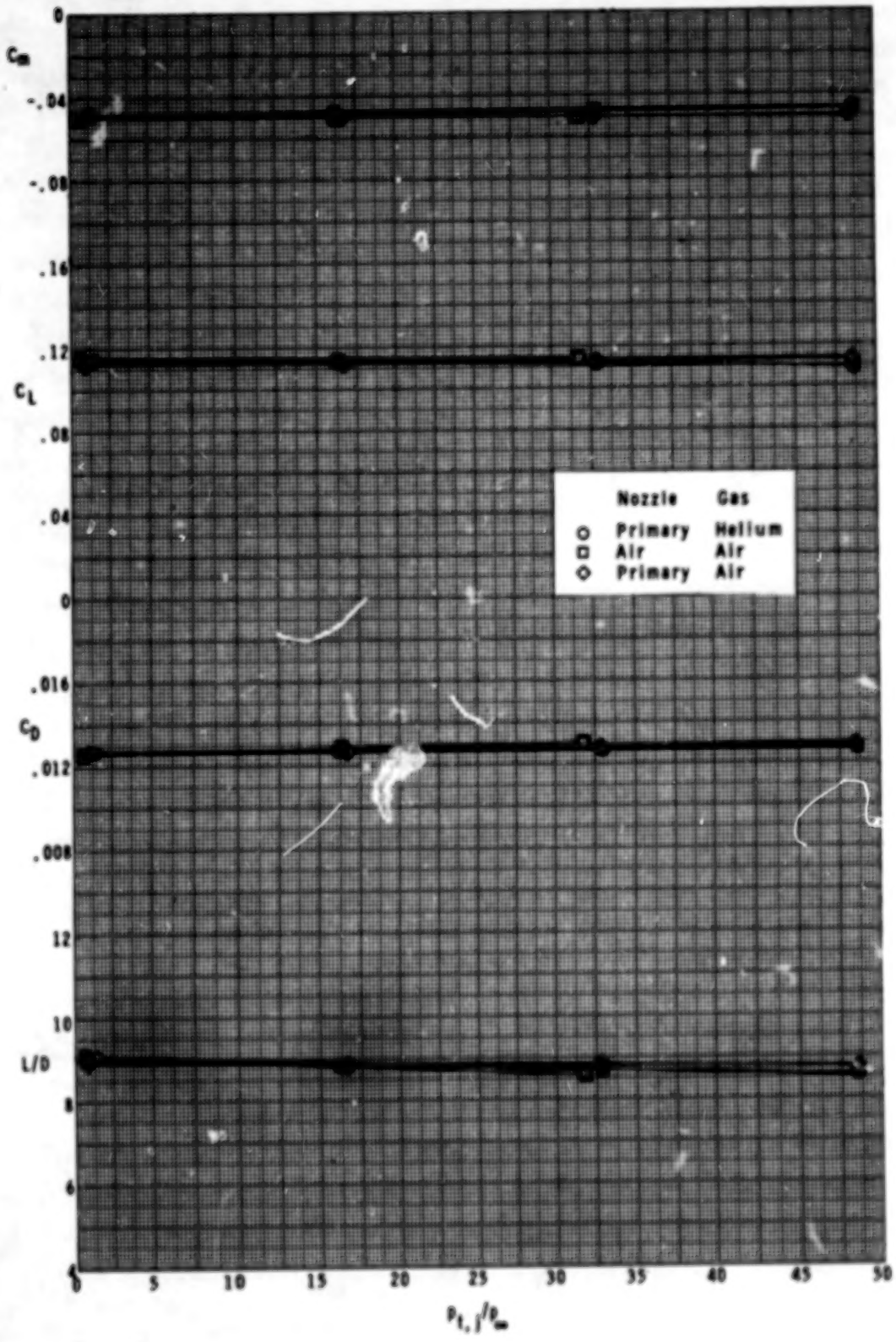

(b) Lower position.

Figure 14.- Concluded.

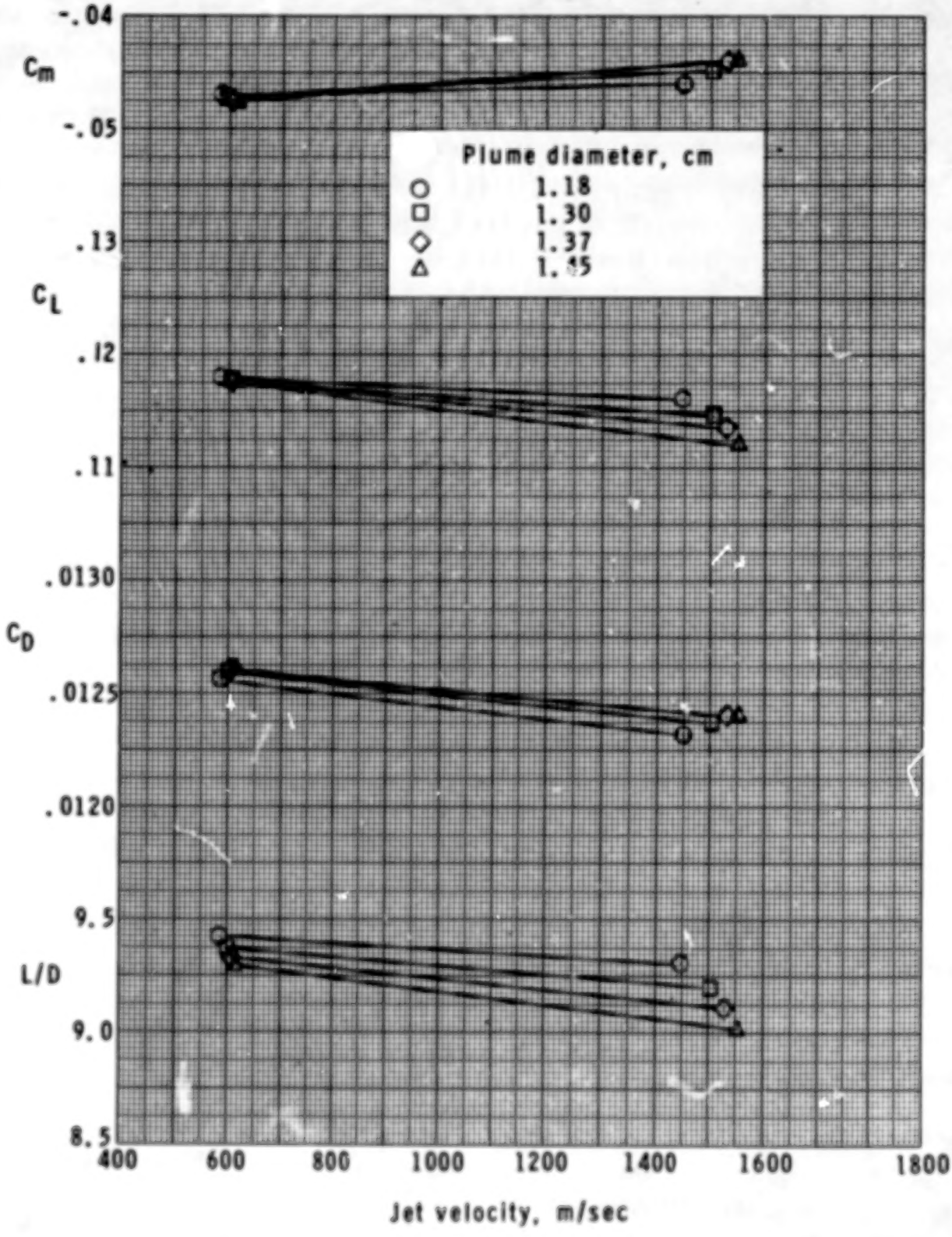

Figure 15.- Variation of longitudinal aerodynamic characteristics of wing with theoretical jet velocity. $\alpha = 2^{\circ}$; upper position.

1. Report No.	2. Government Accession No.	3. Recipient's Catalog No.
NASA TP-1050		

4. Title and Subtitle	5. Report Date
EFFECT OF A SIMULATED ENGINE JET BLOWING ABOVE AN ARROW WING AT MACH 2.0	October 1977
	6. Performing Organization Code

7. Author(s)	8. Performing Organization Report No.
Barrett L. Shrout and Clyde Hayes	L-11751
	10. Work Unit No. 505-11-15-02

9. Performing Organization Name and Address	11. Contract or Grant No.
NASA Langley Research Center Hampton, VA 23665	
	13. Type of Report and Period Covered Technical Paper
12. Sponsoring Agency Name and Address National Aeronautics and Space Administration Washington, DC 20546	14. Sponsoring Agency Code

15. Supplementary Notes

16. Abstract

An investigation of the effects of a gas jet simulating a turbojet engine exhaust blowing above a cambered and twisted arrow wing has been conducted in the Langley 4-foot supersonic pressure tunnel at a Mach number of 2.0. Nozzle pressure ratios from 1 (jet off) to as high as 64 were tested with both helium and air used as jet gases. The tests were conducted at angles of attack from -2° to 8° at a Reynolds number of 9.84×10^{6} per meter. Only the forces and moments on the wing were measured. The results of the investigation indicated that the jet blowing over the wing caused reductions in maximum lift-drag ratio $(L/D)_{max}$ of about 4 percent for helium and 6 percent for air at their respective design nozzle pressure ratios, relative to jet-off data. Moderate changes in the longitudinal, vertical, or angular positions of the jet relative to the wing had little effect on the wing aerodynamic characteristics.

17. Key Words (Suggested by Author(s))	18. Distribution Statement
Over wing blowing Jet exhaust simulation	Unclassified - Unlimited Subject Category 02

19. Security Classif. (of this report)	20. Security Classif. (of this page)	21. No. of Pages	22. Price*
Unclassified	Unclassified	54	$4.50

*For sale by the National Technical Information Service, Springfield, Virginia 22161

NASA-Langley, 1977